International Journal of Medical Microbiology 313 (2023) 151583

Contents lists available at ScienceDirect

International Journal of Medical Microbiology

journal homepage: www.elsevier.com/locate/ijmm

Phenotypic and genotypic discrimination of *Francisella tularensis* ssp. *holarctica* clades

Kristin Köppen [a], Kerstin Rydzewski [a], Joerg Doellinger [b], Kerstin Myrtennäs [c], Mats Forsman [c], Sandra Appelt [d], Holger Scholz [d], Klaus Heuner [a,d,*]

[a] *Working group: Cellular Interactions of Bacterial Pathogens, Centre for Biological Threats and Special Pathogens, Highly Pathogenic Microorganisms (ZBS 2), Robert Koch Institute, Berlin, Germany*
[b] *Centre for Biological Threats and Special Pathogens, Proteomics and Spectroscopy (ZBS 6), Robert Koch Institute, Berlin, Germany*
[c] *Division of CBRN Defence and Security, Swedish Defence Research Agency (FOI), Umeå, Sweden*
[d] *Centre for Biological Threats and Special Pathogens, Highly Pathogenic Microorganisms (ZBS 2), Robert Koch Institute, Berlin, Germany*

ARTICLE INFO

Keywords:
Francisella
Phylogenetic clade B.71
B.12
B.6
Proteomics
Mass spectrometry

ABSTRACT

Francisella tularensis is the causative agent of tularemia, a zoonotic disease with a wide host range. *F. tularensis* ssp. *holarctica* (*Fth*) is of clinical relevance for European countries, including Germany. Whole genome sequencing methods, including canonical Single Nucleotide Polymorphism (canSNP) typing and whole genome SNP typing, have revealed that European *Fth* strains belong to a few monophyletic populations. The majority of German *Fth* isolates belong to two basal phylogenetic clades B.6 (biovar I) and B.12 (biovar II). Strains of B.6 and B.12 seem to differ in their pathogenicity, and it has been shown that strains of biovar II are resistant against erythromycin. In this study, we present data corroborating our previous data demonstrating that basal clade B.12 can be divided into clades B.71 and B.72. By applying phylogenetic whole genome analysis as well as proteome analysis, we could verify that strains of these two clades are distinct from one another. This was confirmed by measuring the intensity of backscatter light on bacteria grown in liquid media. Strains belonging to clades B.6, B.71 or B.72 showed clade-specific backscatter growth curves. Furthermore, we present the whole genome sequence of strain A-1341, as a reference genome of clade B.71, and whole proteomes comparison of *Fth* strains belonging to clades B.6, B.71 and B.72. Further research is necessary to investigate phenotypes and putative differences in pathogenicity of the investigated different clades of *Fth* to better understand the relationship between observed phenotypes, pathogenicity and distribution of *Fth* strains.

1. Introduction

Tularemia, also called “rabbit fever”, is a rare, though re-emerging, potentially severe zoonosis caused by *Francisella tularensis*. This pleomorphic Gram-negative, non-sporulating and non-motile bacterium efficiently proliferates in different host cells, mainly in macrophages (Clemens et al., 2005; Ellis et al., 2002; Keim et al., 2007). The pathogen exhibit a wide host range including mammals, birds, amphibians, fishes, and invertebrates (Ellis et al., 2002; Maurin and Gyuranecz, 2016). Transmission to humans occurs through direct contact with sick animals, as well as animal carcasses, but also through arthropod vectors (mosquitoes and ticks). Transmission through food, drinking water and through environmental sources (water, soil, dust and aerosol) have also been reported (Abdellahoum et al., 2020; Burckhardt et al., 2018; Jacob et al., 2019; Oyston and Griffiths, 2009; Tully and Huntley, 2020). However, despite a case of tularemia after organ transplantation, human to human transmission has not been described so far (Nelson et al., 2019).

In Europe and also in Germany, tularemia is generally caused by the *F. tularensis* subspecies *holarctica* (*Fth*, type-B strains), whereas in North-America, *F. tularensis* ssp. *tularensis* (*Ftt,* type-A strains), *Fth* and *Francisella novicida*, a species rarely pathogenic for humans, are present (Appelt et al., 2020; Champion et al., 2009; Farlow et al., 2005). *F. tularensis* ssp. *mediasiatica* is a further subspecies of *F. tularensis* primarily found in Central Asia, but documented human cases are lacking from the published literature (Challacombe et al., 2017; Öhrman et al.,

* Correspondence to: Cellular Interactions of Bacterial Pathogens, Highly Pathogenic Microorganisms (ZBS 2), Centre for Biological Threats and Special Pathogens, Robert Koch Institute, Seestraße 10, 13353 Berlin, Germany.
E-mail address: HeunerK@rki.de (K. Heuner).

https://doi.org/10.1016/j.ijmm.2023.151583
Received 19 December 2022; Received in revised form 12 June 2023; Accepted 13 June 2023
Available online 14 June 2023

2021). The two clades of *Ftt* (type A.I and A.II), present in North America, differ in their virulence. Type-A.I strains are much more virulent than type-A.II strains (Beckstrom-Sternberg et al., 2007; Farlow et al., 2005; Svensson et al., 2005). For *Fth*, three different biovars have been described: an erythromycin-sensitive biovar I (Ery^S), an erythromycin-resistant biovar II (Ery^R), and biovar *japonica* which is distinguishable by its ability to ferment glycerol (Ellis et al., 2002; Keim et al., 2007). Whole genome sequencing and canonical single-nucleotide polymorphism (canSNP) genotyping methods have revealed multiple *Fth* type clades within this strictly clonal subspecies, including four basal clades B.4, B.6, B.12, and B.16 (Karlsson et al., 2013; Keim et al., 2007; Svensson et al., 2009a; Svensson et al., 2009b; Vogler et al., 2009a; Vogler et al., 2009b). The biovar classification system of *Fth* relates to the canSNP classification system of the bacterium, B.4 and B.6 clades, correlating with Ery^S, the B.12 clade with the Ery^R phenotype, and B.16 with biovar japonica (Karlsson et al., 2016; Kudelina and Olsufiev, 1980; Origgi et al., 2014; Svensson et al., 2009b; Tomaso et al., 2017; Vogler et al., 2009b). Little information is available about further putative phenotypic differences between strains of these basal clades (Hestvik et al., 2018; Karlsson et al., 2016; Kreizinger et al., 2017; Kudelina and Olsufiev, 1980; Origgi et al., 2014; Origgi and Pilo, 2016).

Recently, the phylogenomic analysis of the draft-genome sequences of three isolates from wild animals revealed a new putative clade within the phylogenetic tree of *Fth* (Schulze et al., 2016). The previous B.12/B.13 clade was divided into two sister clades B.71 and B.72. A relatively long branch, leading to isolate A-317 (FDC409) from a raccoon dog (*Nyctereutes procyonoides*), represented B.71. The sister clade B.72, includes all previously known branches within the basal clade B.12 (Schulze et al., 2016) (Fig. 1). In addition, a further new clade (B.75) was identified. It is represented by strain A-271 (FDC408), isolated from a Eurasian beaver (*Castor fiber albicus*) (Schulze et al., 2016) of which the complete genome sequence was recently published (Sundell et al., 2020). During the last few years, various phylogenetic studies of *Fth* isolates from different European countries have been published, demonstrating an unexpectedly high phylogenetic variability within isolates of *Fth,* although *Fth* is strictly clonal with few differences between strains (Appelt et al., 2020; Appelt et al., 2019; Johansson and Petersen, 2010; Kevin et al., 2020; Linde et al., 2020; Mihelcic et al., 2020; Myrtennas et al., 2020; Seiwald et al., 2020; Sundell et al., 2020; Wittwer et al., 2018). Applying core genome MLST and Ridom SeqSphere to 305 sample strains, it was recently demonstrated that the pairwise distance between two isolates was 226.6 SNPs on average and

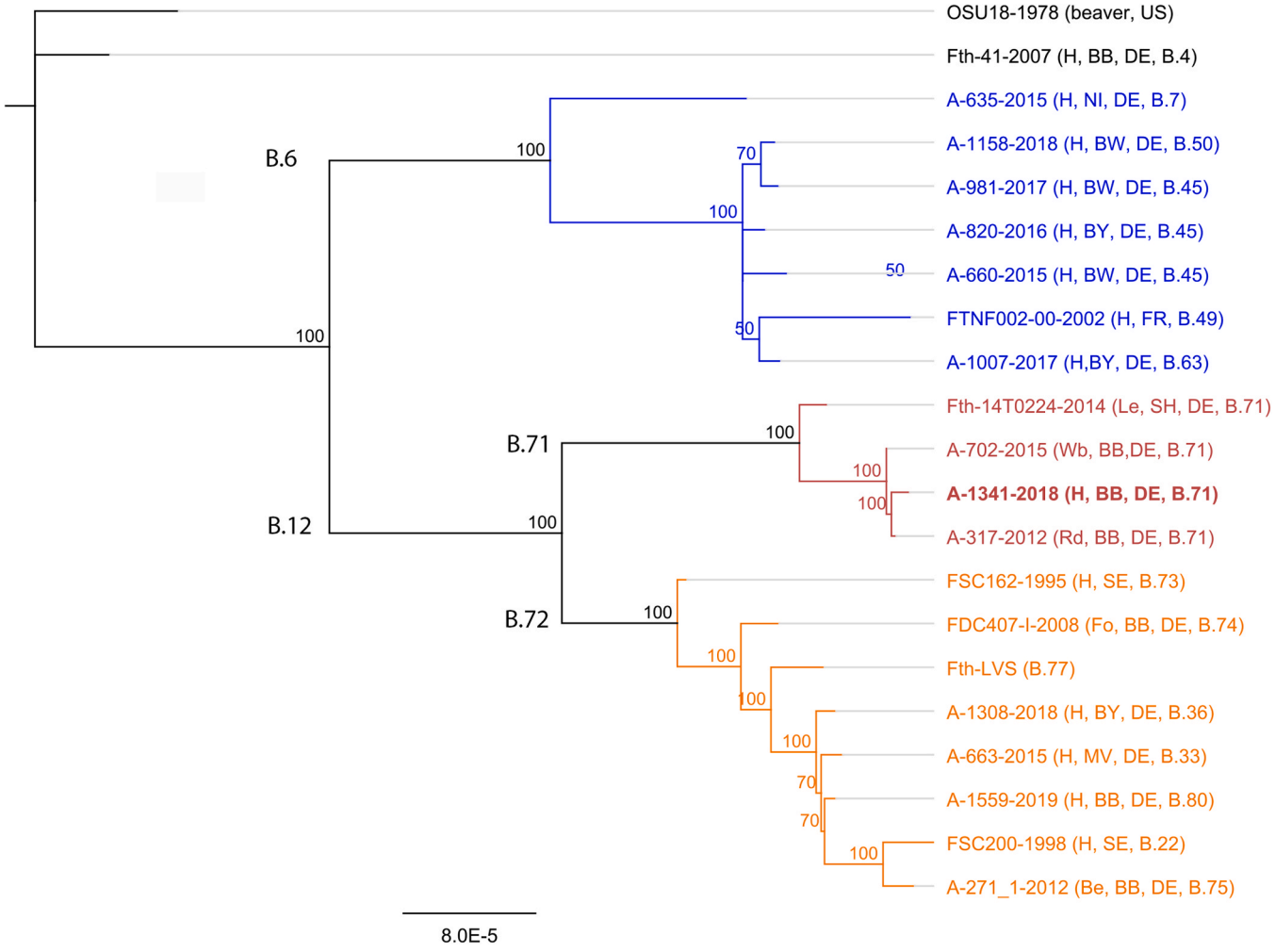

Fig. 1. Phylogenetic tree of selected *Fth* strains. Isolates of clade B.71 (in red) formed a distantly related clade of basal clade B.12 (erythromycin resistant). The isolates belonging to basal clade B.6 are indicated in blue. The analysis was based on a Mauve alignment for colinear genomes. For the clustering, the neighbor joining bootstrap method was chosen, with *F. tularensis* subsp. *holarctica* strain OSU18 as an out-group. Substitutions per site are indicated (line below the tree). For each genome, the identifier of the isolate and the year of sampling, the host organism, the sampling spot (federal state, Germany), and the respective *Francisella* clade or final clade for each genome is given. Abbreviations: US, United States, FR, France; SE, Sweden; Germany's federal states: BB: Brandenburg; BW: Baden-Württemberg, BY: Bavaria; MV: Mecklenburg-Western Pomerania; NI: Lower Saxony; SH: Schleswig-Holstein; Be, beaver; Fo, fox; H, human; Le, Lepus; Rd, racoon dog; Wb, wild boar. The genome sequences of the isolates used here have been published earlier (Appelt et al., 2019).

ranged from 0 to 490 SNPs (Linde et al., 2020). However, a study from Sweden showed a mutation rate of nearly zero. Only in outbreak hotspots, the rate rose up to 0.4 mutations/genome/year (Dwibedi et al., 2016).

The identification of a new B.12 clade named B.71 in the Berlin/Brandenburg area that was only distantly related to all other strains previously found within basal clade B.12, revealed gaps of knowledge regarding the phylogeography of *Fth.* We, therefore, sequenced further genomes of *Fth* isolates from all over Germany to be able to fill these gaps (Appelt et al., 2020; Appelt et al., 2019; Faber et al., 2018), and identified four members of clade B.71 (see below).

An easy way to identify basic phenotypical differences between bacteria strains is to monitor growth in liquid media. The backscatter light measurement method is used to investigate growth and growth rates of microorganisms in liquid media (Bruder et al., 2016; Hemmerich et al., 2017). An automated system continuously monitors the biomass (and growth rates) in shaking flask cultures in a non-invasive and parallelisable manner. The backscattering intensity depends on the morphology and size of the investigated cell, but is also able to detect diauxic shifts (metabolism) during growth (Bruder et al., 2016). In general, backscattering intensity increases with decreasing particle volume (Latimer and Pile, 1972). The method allows an efficient growth-based characterization of microorganisms and also enables the comparison of mutant strains for biological fitness evaluations (Bruder et al., 2016; Hemmerich et al., 2017).

The aim of this study was to genotypically and phenotypically characterise the clades B.6, B.71 and B.72, and to provide a reference genome of the new clade B.71 (Appelt et al., 2019; Schulze et al., 2016), using strain *Fth* A-1341. The strain was isolated from a patient suffering from tularemia after contact with a wild boar during a hunt in Berlin-Brandenburg, Germany, in 2018. Yet, there are only three further isolates of clade B.71: A-317 (from a raccoon dog, 2012), A-702 (from a wild boar, 2005), also isolated in Berlin-Brandenburg from hunted wild animals (Schulze et al., 2016), and 14T0224, isolated from a hare (*Lepus europaeus*, 2014) in Schleswig Holstein, Germany (Linde et al., 2020). When used in this study, these were freshly isolated, only being passaged a few times on agar plates. Further, the strains of clade B.71 were investigated for different and common features in their genome sequences (SNPs; putative canSNPs, InDels; pseudogenes) and for phenotypic differences in strains of clade B.71 in comparison to isolates of clades B.72 and B.6, respectively.

2. Materials and methods

2.1. Bacterial strains, growth conditions and growth measurement

Strains used in this study were *Fth* isolates (A-1341, A-702, A-317, A-1559, A-663, A-1308, A-1007, A-820, A-981, A-1158, A-660) from Germany, including isolates from humans and free-living animals (Appelt et al., 2019) (see also Fig. 1).

Francisella strains were cultivated in medium T (Becker et al., 2016; Pavlovich and Mishan'kin, 1987), Chamberlain's chemically defined medium (CDM) (Chamberlain, 1965), and medium T-based agar plates (MTKH plates: medium T supplemented with 2.4 g l^{-1} of activated charcoal, 9.5 g l^{-1} of hemoglobin and 14.3 g l^{-1} of agar) (Tlapak et al., 2018) at 37 °C.

Bacterial growth (biomass, culture density) was measured by Cell Growth Quantifier (CGQ, Aquila BioLabs, Beasweiler, Germany) or by measurement of the optical density (OD_{600}) using a photometer (Genesys 10 bio, Thermo Scientific, Germany).

Volumes of 20 ml of medium T or CDM were inoculated with an over-night culture of the *Francisella* strains leading to a final OD_{600} of 0.3. Culture flasks were incubated at 37 °C and 250 rpm. One flask was used to determine backscatter values (as "scattered light intensity") automatically every hour of incubation by CGQ (Bruder et al., 2016). A second flask served to determine the optical density at 600 nm (OD_{600}) and colony forming units (CFU) at selected time points.

2.2. Phylogenetic analysis

The consensus sequences of genomes were extracted and aligned using a progressive Mauve alignment for collinear genomes applying the Muscle (version 3.6; (Edgar, 2004)) alignment algorithm in Geneious Prime (Version 2020.2.3) (Kearse et al., 2012). The alignment was used for phylogenetic constructions. The construction of the phylogenetic tree was based on entire (draft) genome sequences. To generate the phylogenetic tree through the neighbor joining method for clustering, Geneious Prime was used applying a bootstrap of 100 (Saitou and Nei, 1987). Reference genomes included in the phylogenetic reconstructions were *F. tularensis* subsp. *holarctica* OSU18 (NCBI Reference: NC_017463.1), *F. tularensis* subsp. *holarctica* LVS (NCBI Reference: NC_007880.1), *F. tularensis* subsp. *holarctica* FSC162 (NCBI Reference: PRJNA89145), *F. tularensis* subsp. *holarctica* FSC200 (NCBI Reference: NC_019551.1) and FTNF002–00 (NCBI Reference: NC_009749.1).

2.3. SNP, Indel and pseudogene analysis

SNPs and Indels were extracted from a genome sequence alignment of *Fth* OSU 18 (NCBI reference NC_017463.1), *Fth*-41 (B.4), 45 B.6 strains, 25 B.72 strains and four B.71 strains using Geneious Prime and manual inspection. Identification of pseudogenes was done by using Geneious Prime and Artemis (Release 7, Sanger Institute).

2.4. PCR and Sanger sequencing

PCR was carried out using a Thermocycler TRIO-Thermoblock (Biometra, Göttingen, Germany) and the TopTaq DNA polymerase (Qiagen, Hilden, Germany). In general, initial denaturation was performed at 94 °C for 3 min, whereas final extension was performed at 72 °C for 10 min. Using ~ 100 ng of template DNA, the cycling conditions (35 cycles) were 94 °C for 30 s, 57 °C for 1 min and 72 °C for 1 min. Obtained PCR product were used for Sanger sequencing (LI-COR-DNA4000; MWG-Biotech, Ebersberg, Germany). Oligonucleotides were obtained from Eurofins MWG Operon (Ebersberg, Germany).

2.5. Genome sequencing and assembly of a complete genome sequence

DNA was extracted by MagAttract (Qiagen GmbH, Germany) and amplified by REPLI-g MIDI kit (Qiagen GmbH, Germany). The sequencing library was prepared with Nextera XT DNA sample prep kit v3 (Illumina Inc., USA) with 600 cycles. For the MinION sequencing platform, the amplified DNA was endonuclease treated with T7 endonuclease I (New England Biolabs, Ipswich, MA, USA). The whole genome sequencing library was prepared using Oxford Nanopore SQK-LSK108 kit protocol with the native barcoding expansion kit EXP-NBD103 and sequenced on a flow cell with R9.4 chemistry MIN106. No DNA size selection or fragmentation was performed prior to sequencing. Whole genome sequencing was performed on both, MiSeq instrument (Illumina Inc., USA) and MinION instrument (Oxford Nanopore Technologies Ltd, UK), generating 4164,480 trimmed pair-end read pairs (median read length 222 bp; 35–301 bp) and 424,221 long reads (median read length 1763 bp, read length N50 4027 bp). Illumina reads were trimmed using Trimmomatic (v.0.36; LEADING:3, TRAILING:3, SLIDINGWINDOW:4:15, MINLEN:36) removing low quality bases at the end of reads (Bolger et al., 2014). Nanopore reads were base-called using Albacore (v2.1.3) (https://community.nanoporetech.com), and adapters were trimmed with Porechop (v.0.2.3_seqan2.1.1). A polished linear sequence was generated with the hybrid assembler Unicycler (v.0.4.7), using both, short Illumina reads and long Nanopore reads, as input (Wick et al., 2017). In addition, the two expected copies of the 30 kbp *Francisella* pathogenicity island (FPI), the IS element containing regions, and the circular form of the genome were resolved by mapping

Nanopore reads longer than 15 kbp (41,208 sequences) back to the obtained draft genome sequences using Geneious mapper and manual inspection. Ambiguous genome regions were amplified by PCR and sequenced by LI-COR sequencer to confirm identity and correct assembly. Finally, the genome was rotated to start with *dnaA*. Annotation was performed by the NCBI Prokaryotic Genome Annotation Tool (https://www.ncbi.nlm.nih.gov/genome/annotation_prok/) (Li et al., 2021). The 1893,440 bp circular chromosome of A-1341 has a GC content of 32.2%.

2.6. Data availability

The European Archive lists the first draft version of the A-1341 genome sequence under accession no. PRJEB33006 and SAMEA5971373 (Appelt et al., 2019). The final genome sequence of strain A-1341 has been deposited in GenBank under the accession no. CP098826.1.

2.7. Proteome analysis

2.7.1. Sample preparation for proteomics

For proteomic analysis *Fth* strains were cultivated on MTKH agar plates at 37 °C and 5% CO_2 for 24 h. Sample Preparation by Easy Extraction and Digestion (SPEED) (Doellinger et al., 2020) was used to prepare the samples. Briefly, colony material was transferred into 130 µl of trifluoroacetic acid (TFA) (Thermo Fisher Scientific, Waltham, MA, USA) and incubated at room temperature for 15 min. For neutralization (pH = 8), 100 µl of sample-TFA-solution was transferred into prepared reaction tubes containing 1 ml of 2 M TrisBase. The reduction buffer (tris(2-carboxyethyl)phosphine (TCEP) - final concentration of 10 mM, and 2-Chloroacetamide (CAA) - final concentration of 40 mM) was added, and samples were incubated at 95 °C for 5 min. Protein concentration was measured using turbidity measurements on a UV–VIS spectrophotometer (Implen NP80 spectrophotometer (Implen, Munich, Germany)), and samples were adjusted to 0.5 µg/µl with sample dilution buffer (SDB, 10:1 mixture of 2 M TrisBase: TFA). 100 µl of this solution was diluted 1:5 with water and digested with 2 µg of Trypsin Gold, MS Grade (Promega, Fitchburg, WI, USA) at 37 °C. After 20 h, resulting peptides were acidified with TFA (final concentration 2%, pH = 2) and centrifuged (8000 x g, 2 min). Peptides were desalted using Pierce™ Peptide Desalting Spin Columns according to the manufacturer's instructions and dried by a vacuum concentrator. Dried peptides were resuspended in 40 µl 0.1 FA. Peptide concentration was determined using Implen NP80 spectrophotometer (Implen, Munich, Germany).

2.7.2. Liquid chromatography and mass spectrometry

Peptides were analyzed on an EASY-nanoLC 1200 (Thermo Fisher Scientific, Bremen, Germany) coupled online to a Q Exactive™ HF mass spectrometer (Thermo Fisher Scientific). 1 µg of peptides were separated on a PepSep column (15 cm length, 75 µm i.d., 1.9 µm C18 beads, PepSep, Marslev, Denmark) using a stepped 30 min gradient of 80% acetonitrile (solvent B) in 0.1% formic acid (solvent A) at 300 nl/min flow rate: 5–11% B in 2:49 min, 11–29% B in 18:04 min, 29–33% B in 3:03 min, 33–39% B in 2:04 min, 39–95% B in 0:10 min, 95% B for 2:20 min, 95–0% B in 0:10 min and 0% B for 0:50 min. Column temperature was kept at 50 °C using a butterfly heater (Phoenix S&T, Chester, PA, USA). The Q Exactive™ HF was operated in a data-independent (DIA) manner in the *m/z* range of 345–1650. Full scan spectra were recorded with a resolution of 120,000 using an automatic gain control (AGC) target value of 3×10^6 with a maximum injection time of 100 ms. The full scans were followed by 56 DIA scans of dynamic window width using an overlap of 0.5 Th. DIA spectra were recorded at a resolution of 30,000 using an AGC target value of 3×10^6 with a maximum injection time set to auto and a first fixed mass of 200. The normalized collision energy (NCE) was set to 27%, and default charge state was set to 3. Peptides were ionized using electrospray with a stainless steel emitter, I.D. 30 µm (PepSep) at a spray voltage of 2.1 kV and a heated capillary temperature of 275 °C.

2.7.3. Data analysis

Consisting of peptides derived from proteomes - obtained from UniProt - of *Fth* FDC408 (A-271_1), belonging to clade B.72, *Fth* A-1341 to B.71 and *Fth* FTNF002–00 to B.6, a spectral library was predicted using the deep-learning algorithm implemented in DIA-NN (version 1.8) (Demichev et al., 2020). A strict trypsin specificity (KR not P) allowed up to one missed cleavage site in the *m/z* range of 350 – 1150 with charge states of 2 – 4 for all peptides consisting of 7–30 amino acids with enabled N-terminal methionine excision and cysteine carbamidomethylation. The mass spectra were analyzed in DIA-NN (version 1.8) with fixed mass tolerances of 10 ppm for MS1 and 20 ppm for MS^2 spectra allowing a "matched between run" option. The false discovery rate was set to 0.01 for precursor identifications, and proteins were grouped using the relaxed inference strategy. The resulting pg_matrix.tsv (protein FDR = 1%) file was used for further analysis in Perseus (version 1.6.5). Relative protein quantification was based on log (2)-transformed and Z-score normalized "MaxLFQ" intensities. Proteins, which were not quantified in at least 2 out of 3 replicates of one sample, were removed, and remaining missing values replaced from a normal distribution (width 0.3, downshift 1.8). Significant protein expression differences between samples were identified using an ANOVA test with a permutation-based FDR of 0.05 (250 randomizations, s0 = 0.1). Subsequently, a post-hoc test was applied to detect significant sample pairs using an FDR of 0.05. Protein expression differences between clades were analysed using t-tests with FDR 0.01, 250 randomizations and s0 = 1.

The mass spectrometry proteomics data have been deposited to the ProteomeXchange Consortium (http://proteomecentral.proteomexchange.org) via the PRIDE partner repository with the dataset identifier PXD038948.

3. Results

3.1. The genome sequence of strain A-1341 was completed and selected as a reference genome for Fth clade B.71

We previously identified a new clade (B.71) within basal clade B.12 (Schulze et al., 2016). The human isolate *Fth* strain A-1341, a member of clade B.71 was genome sequenced, and selected as a reference strain of clade B.71. The 1,893,440 bp circular chromosome of strain A-1341 has a GC content of 32.2%, with 1942 total CDS, 1709 CDS (with protein), 1994 total genes, 10 rRNAs, 38 tRNAs, 2 regulatory RNAs, one mtRNA and 3 noncoding RNAs. The genome sequence showed the SNPs in the *rrl* (23 S rRNA) gene (A453G and A2059C, *E. coli*) which have been found to be responsible for erythromycin resistance of all strains of basal clade B.12 in a previous study (Karlsson et al., 2016).

3.2. Strain A-1341 specific differences

Homologues of known virulence genes of *F. tularensis* are present in the genome sequence of strain A-1341. The strain exhibits 12 SNPs and one nucleotide deletion (T), none of which is present in isolates A-317, A-702 or 14T0224 (Table 1 A), also members of the new clade B.71 (Fig. 1, strains indicated in dark red). The strain specific "T" base deletion of A-1341 is located within the IS630 (ISFtu1) element. Although the strain specific SNPs are located within genes, these did not lead to a stop codon or a frame-shift, for details see Table 1 A. However, in two supposed proteins the respective SNP led to conversions of a nonpolar to a polar amino acid (IS5 family transport protein, Table 1 A, no. 10) and of a polar to a basic amino acid (HAMP domain containing histidine kinase, Table 1 A, no. 12).

Table 1
A: A-1341 specific SNPs and Indels.

No.	Gene/Protein (NF101_00000)	NT position	SNP/ Indel	Function/Description
1.	*radA* (01895)	346,460	T (C)	I (V), DNA repair protein RadA
2.	(02080)	380,326	T (G)	I (V), HP
3.	(02750)	514,141	T (C)	T (T), sugar binding protein
4.	*lpoB* (02950)	551,807	G (A)	V (I), PBP activator protein LpoB
5.	(03345)	633,332	C (A)	R (L), pro-tRNA ligase
6.	*sthA* (04895)	930,839	T (C)	N (D), si-specific NAD(P) transhydrogenase
7.	*lptB* (05450)	1,019,890	A (G)	I (M), LPS export ABC TP ATP-BP
8.	*dxs* (05480)	1,028,500	A (G)	S (G), deoxy-D-xylulose-5-P synthase
9.	(07445)	1,383,378	T (C)	H (R), DNA-3-methyl-adenine glycosylase
10.	Is5 Tp (07645)	1,429,184	C (T)	L (T), Is5 family transport protein
11.	(08535)	1,616,006	A (G)	S (S), multidrug efflux MFS transport protein
12.	(08950)	1,694,109	T (G)	S (R), HAMP domain containing His-kinase
13.	IS630	multiple	T del	Transposase, IsFtu1

3.3. Clade B.71 specific differences affected genes involved in replication, metabolism and outer membrane stability

The analysis of the four strains belonging to phylogenetic clade B.71 revealed a canSNP (C -> T) at position 473 of the 16 s rDNA gene (1523 bp) in each of the three copies present in the genome (Table 1B, no. 23). In summary, we identified 245 specific SNPs, six of which leading to pseudogenes, as well as 24 B.71 specific Indels of 1–16 nucleotides in length (Table 1B). 12 of the Indels presumably led to the inactivation of the respective genes (generating pseudogenes) encoding metabolic function (4x), membrane (function) proteins (5x), DNA replication and repair (DNA polymerase III, DNA polymerase IV and a putative helicase), as well as a protein prior identified as a virulence factor of *Francisella* (MlaA/VacJ). Further 11 of these Indels are found in intergenic regions (for details, see Table 1B).

3.4. B.72 specific deletions

In addition, we identified seven B.72 clade-specific deletions (1–11 NT in length), not known to be present in strains of clade B.71 (Table 2), although they are members of basal clade B.12. Four of these deletions are found in pseudogenes, two in intergenic regions and one within a protein encoding gene (NF101_09335) coding for a putative GDSL-like lipase or esterase. The lipase seems to be inactivated in the B.72 strains.

Table 1B
Clade B.71 specific Indels (frame-shift) or stop codons.

No.	Gene (NF101_)	NT position	SNP/Indel	Function/Description
1.	Int-region (————)	25	C del	
2.	Int-region (————)	91,947	T del	
3 * /°.	DUF3573 (00735)	153,796	TGTTATC del	Putative siderophore uptake, SP
4 * /°.	(00945)	186,859	C del	periplasmic substrate-binding protein, SP
5.	Int-region (————)	251,610	TTTCTACAAAT ATCTT in	
6.	Int-region (————)	335,361	ACATT in	End of prepilin cleavage protein
7°.	Is5 Tp (02230)	411,871	AA in	Transposon
8 * /°.	*SUA5/yrdC* (02235)	411,971	GAAATTGG del	Unknown function
9°.	DUF2254 (02420)	447,543	A in	Elongated protein, predicted membrane protein
10.	P-region (02425)	447,812	AAAT del	dnaE, DNA polymerase III subunit alpha
11 * /°.	*asd* (02540)	482,110	A del	aspartate-semialdehyde dehydrogenase
12.	Int-region (————)	508,984	T in	
13°.	HP (02890)	543,757	C del	DUF3833,
14 * /°.	*xylE* (03000)	561,321	T in	Putative D-xylose transporter, sugar-TP
15 * /°.	(03625)	692,256	T(G)	Stop codon, -> ps-gene FAD binding oxidoreductase
16.	HP (03630)	692,553	A(T)	Stop codon, CDS two Aa shorter SP, putative lipoprotein
17 * /* */°.	*mlaA* (03990)	756,392	TTTGTTG del	Lipoprotein, asymmetry of the outer membrane, (*vacJ*)
18.	Int-region (————)	888,400	ATAATGACTTA del	
19 * /°.	Ps-gene (04830)	918,517	T del	MFS transporter
20#.	P-region (04980) of *pmrA*	945,841	AGTTTT del	In front of *pmrA* (50 S ribosomal protein L11 methyltransferase)
21 * /°.	*dusB* (04985)	947,351	T(G)	Stop codon, -> ps-gene, tRNA dihydrouridine synthase
22 * /°.	*dinB* (05020)	953,990	TCTAC del	DNA polymerase IV, induced in SOS response, 3′→5′ exonuclease
23.	16 S rDNA (00610) (02270) (05985)	125,138 418,155 1,121,732	T(C)	16 S rRNA
24.	Int-region (————)	1,308,029	AAATTAAT del	In front of 06730
25 * /°.	HP (06215)	1,166,525	TA in	CDS, alternative, two Aa shorter
26 * /°.	Ps-gene (08005)	1,502,718	TTC del	DUF2147
27.	Int-region (————)	1,524,455	T in	In front of *lptD*
28 * /°.	(08905)	1,685,385	T (G)	Stop codon, AAA family ATPase; DEAD-like helicases superfamily
29.	Int-region (————)	1,831,357	TTTA del	
30 * /°.	HP (09700)	1,847,023	A(G)	Stop codon, DUF4131 domain containing protein

Aa, amino acid; BP, binding protein; HAMP domain, present in Histidine kinases, Adenylate cyclases, Methyl accepting proteins and Phosphatases; HP, hypothetical protein; Int, intergenic; P, promotor; PBP, Penicillin binding protein; Ps, pseudogene; SP, signal peptide; TP, transport protein
* putatively inactivated by clade B.71 specific frame-shift or stop codon, (-> pseudo (ps)-gene)
° not detected in proteom of A-1341
* * known virulence factor
is not B.71 specific, deletion also present in *Ftt* (SchuS4, FSC198)

Table 2
Clade B.72 specific deletions, not present in strains of clade B.71.

No.	Gene (NF101_00000)	NT position	Deletion	Function/Description
1.	Ps-gene (00325)	65,285	ATAA	Putative glycosyl hydrolase
2.	Ps-gene (04175)	800,155	TTTCAAGTTCA	Putative galactose mutarotase, lactose metabolism, SP
3.	Ps-gene (04300)	820,769	TAA	Aa transport protein
4.	Int-region (————)	1,488,249	TTTAA	
5.	Int-region (————)	1,528,801	T	
6.	Gene (09335)	1,771,183	T	GDSL-like lipase or esterase, ps-gene in B.72
7.	Ps-gene (09865)	1,877,683	A	LysE family transport protein

3.5. Members of clade B.71 exhibit common specific phenotypes

Since we identified various B.71 specific mutations in different genes (see above), we investigated if strains of clade B.71 show similar phenotypes.

3.5.1. The investigated backscatter growth phenotype differs from that of clades B.6 and B.72 in both medium T and CDM

First, we investigated the growth behaviour of three *Fth* strains (A-271 (B.72, red), A-660 (B.6, blue) and A-1341 (B.71, green), Fig. 2) in complete medium T and in CDM by the backscatter method (Bruder et al., 2016; Kensy et al., 2009). In addition, we measured OD_{600} and determined the CFU, for medium T at 0 h, 20 h and 24 h of incubation and for CDM at 0 h, 8 h and 24 h. Results are given in Fig. 2. In general, the observed backscatter intensity (Fig. 2 A), could be verified by OD_{600} (Fig. 2B) and CFU (Fig. 2 C) values, indicating that this method is apt to investigate the growth of *Francisella* in liquid medium. For example, in medium T, backscatter values (Fig. 2 A) as well as values of OD_{600} (Fig. 2B) and CFU (Fig. 2C) increased for strain A-1341 between 20 and 24 h. In addition, for both media, the experiments revealed the tendency of perceptible differences in the obtained overall backscatter growth curves of the strains investigated.

Therefore, we investigated if strains of the different clades (B.6, B.71 and B.72) showed a clade-specific growth phenotype. The following strains of the clades were selected: basal clade B.6, strains A-660 ([B.45], A-1007 [B.46/B.63], A-1158 [B.45/B.50], A-820 [B.45], A-981 [B.45]; clade B.72, A-271 [B.75], A-1559 [B.33/B.80], A-663 [B.33], A-1308 [B.34/B.36]) and the three available strains of B.71 (A-1341, A-317 and A-702) and were grown in medium T (see Fig. S1A, n = 2–8 for each strain, total experiments: 18 x B.71, 16 x B.72, 19 x B.6) and CDM (see Fig. S1B, n = 3–12 for each strain, total experiments: 18 x B.71, 19 x B.72, 12 x B.6), respectively. Backscatter analysis of clade-specific growth are shown in Fig. 3. In this figure, 10 backscatter curves (from three different strains) were included in the growth curve shown for each clade. In contrast to strains of basal clade B.6 or of clade B.72, the results revealed that isolates belonging to clade B.71 exhibit a common backscatter growth curve in both media used for investigation. In medium T, for example, for strains of B.71 backscatter values increased from 20 to 24 h of incubation and strains of clade B.6 exhibit a decrease of backscatter values between 5 and 6 h of incubation, not present in the other strains investigated (Fig. 3A), whereas the shape of the backscatter curve of strains of clade B.72 are similar to a typical growth curve (OD_{600}). Although these differences are not statistically significant, the overall backscatter growth curve of strains belonging to the same clade are discriminable from the other strains investigated (see also supplemental Fig. S1). For growth in CDM, at the end of exponential growth (9–10 h), backscatter values for strains of clade B.71 were lower than in strains of clade B.6 and B.72 (Fig. 3B, Fig. S1B). A common and clade-specific backscatter trend was also found for strains of clade B.72, characterized by a decrease of backscatter values after 13–16 h of incubation (Fig. 3B, Fig. S1B). Strains belonging to basal clade B.6 revealed higher backscatter values in the exponential growth phase (6–11 h) and in the late stationary phase (after 15 h, Fig. 3B and supplemental Fig. S1B). Thus, all strains belonging to a specific clade investigated here showed a common shape of the overall backscatter curve produced by the CGQ method.

Since the B.71 strains showed clade-specific mutations in genes encoding putative proteins involved in the metabolism (aspartate-semialdehyd dehydrogenase, oxidoreductase, MFS and sugar transport proteins) or in outer membrane stability (MlaA, membrane protein, lipoprotein), we investigated the growth of our strains in CDM and in specifically modified CDM (CDM without aspartate or arginine; without glucose, but with xylose or galactose). Although no significant differences between strain A-1341 (B.71) and A-271 (B.72) could be observed, the results confirm the assumption that glucose and arginine are essential for successful growth in CDM for both strains (data not shown).

3.5.2. Whole proteome analysis complements findings of the phylogenetic genome analysis

In the phylogenetic analysis of whole genomes, strains of clades B.6 and B.12, as well as B.71 and B.72 formed different phylogenetic clusters (see Fig. 1). Here, we performed a whole-cell comparative proteomic analysis using LC-MS/MS of three strains of each clade (B.6, B.71 and B.72; n = 3), respectively (Fig. 4). Whole cell proteomic approaches provide a global view on the abundance of the proteins expressed during growth. Whole cell protein samples were prepared from bacteria grown on MTKH agar plates at 37 °C. Each strain was analyzed in three independent biological replicates (see Materials and Methods). A common set of proteins was expressed in a basal clade or basal clade-specific pattern (Fig. 4). In total, 1349 homologous proteins were detected representing 79% of annotated CDS (with protein) of *Fth* A-1341 (see 3.1). Fourteen genes were identified as putative pseudogenes, either because of stop codons or deletions leading to frame shift (Table 1B). The genomic sequence analyses were confirmed, when none of these genes were found to be expressed in *Fth* A-1341 under tested conditions. Genes possessing B.71-specific Indels within its putative promotor region (*dnaE*, *pmrA* and *lptD*, Table 1B, Fig. 4) are highlighted in Fig. 5. B.71 strains possessed a higher abundance of 250 proteins compared to strains belonging to B.6 clade and 69 compared to B.72 (FDR 0.01, s0 = 1, Fig. 5, supplemental Tab. S1). Selected proteins are listed in Table 3. On the other hand, 309 and 98 proteins, respectively, were significantly lower expressed in B.71 compared to B.6 and B.72, respectively. Selected proteins are listed in Table 4. Many proteins involved in the biotin metabolism, such as BioJ (BioH), BioA, BioB and BioD, are significantly lower expressed in B.71 than in B.72 and B.6. From totally 1349 identified homologous proteins, 745 proteins were significantly differently expressed (FDR 1%, s0 = 1, supplemental Tab. S1, Fig. 4). These were used to generate a HeatMap illustrating a specific abundance pattern for B.71, B.72 and B.6 strains with fold changes between − 2.4 and 2.5. Three clusters specific for B.71 were identified. Cluster 1 and 2 comprise 21 and 17 proteins, respectively, which were significantly higher expressed in B.71. Both clusters consist of diverse proteins which are involved in metabolic pathways (f.i. PurB, DoeC), DNA repair (MutS) and composition of the bacterial cell envelope (BamA, SecA, SecD). Also, virulence-associated proteins are present within both clusters, such as CarA, PdpA GalU and FkpB. Within cluster 3, 103 proteins were identified that are lower expressed in B.71 strains compared to B.6 and B.72 strains. This cluster contains also a diverse protein group including ribosomal proteins (PrmA, RsmA), DNA-replication/repair proteins (DnaE, UvrB), transporter (LptF, FupA, TrkA), metabolic proteins (SerC, PlsX) and proteins involved in biotin biosynthesis (BioA, BioB, BioD, BioJ). Here, also several virulence-associated proteins were found, including PilQ, ClpB and SdhA.

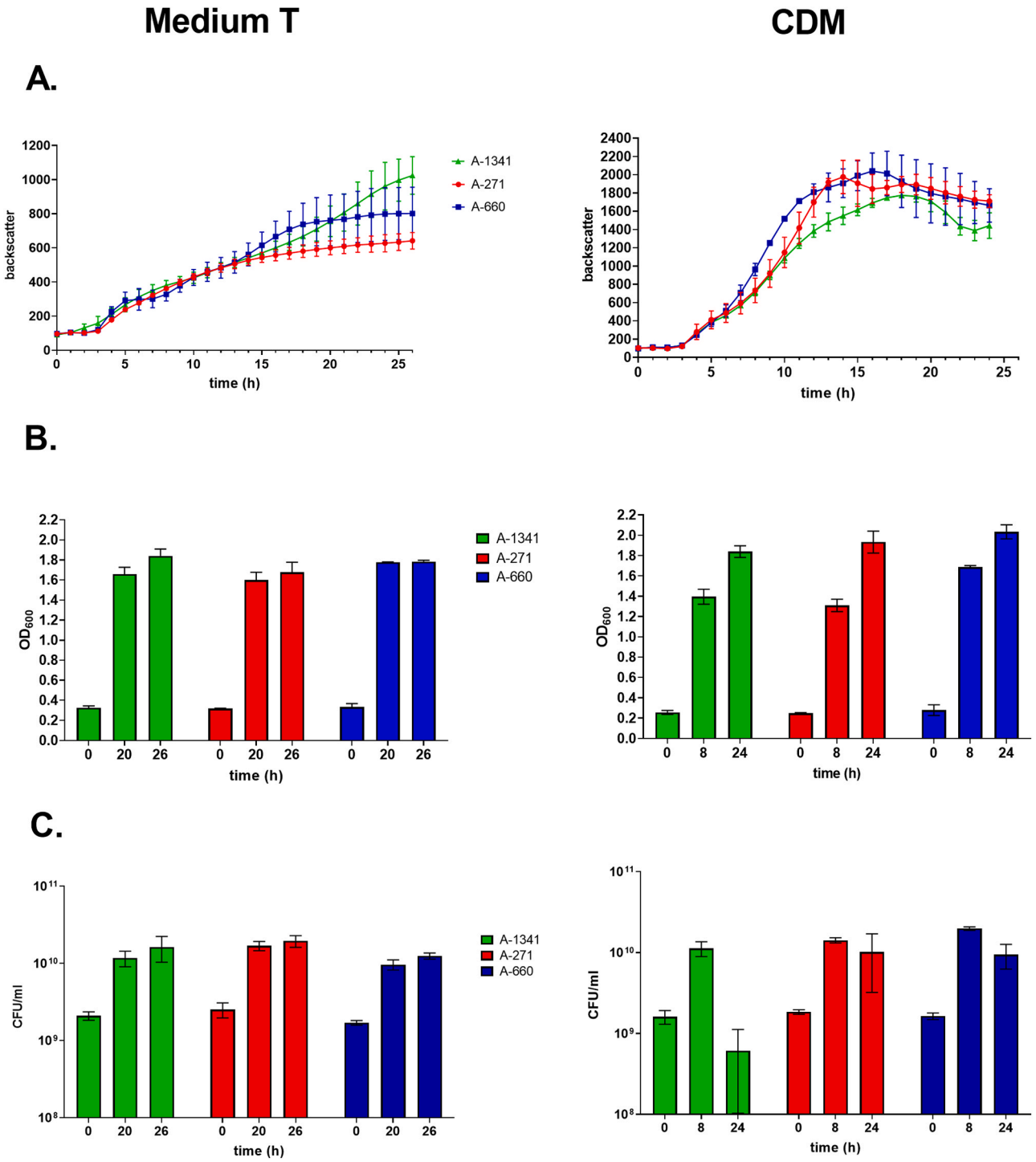

Fig. 2. Growth behavior of *Fth* strains A-1341 (B.71), A-271 (B.72) and A-660 (B.6) in medium T and CDM analyzed by the measurement of backscatter (A), OD_{600} (B) and colony forming units on agar plates (C). A. Bacteria were incubated with rotation at 37 °C up to 25 h. Backscatter values were measured each hour. Shown are the means with standard deviation; n = 3 (medium T), n = 2 (CDM). B. and C. At 0 h, 20 h and 26 h (Medium T) and at 0 h, 8 h and 24 h (CDM) of growth OD_{600} values were measured and bacteria were plated out onto agar plates to determine the CFU. Results are mean values with standard deviation of two independent experiments: blue, A-660 (B.6); red, A-271 (B.72); green, A-1341 (B.71).

Although the protein abundance pattern was more similar between B.71 and B.72 strains (as expected, Figs. 4 and 5), some proteins showed abundances similar to B.6 strains (yellow square in HeatMap, Fig. 4). This cluster included 21 proteins (f.i. RplM and NuoI) which were found in a lower abundance in B.6 and B.71 than in B.72.

In summary, the proteome pattern of differently expressed genes of isolates from strains of basal clades B.6 and B.12 clusters as separate branches, but also strains of clades B.71 and B.72 cluster as different branches (see Fig. 4). Thus, we could demonstrate the presence of a clade-specific proteome pattern in strains of *Fth*.

4. Discussion

In Europe, basal clades B.6 and B.12 of *Fth* are present. In Germany,

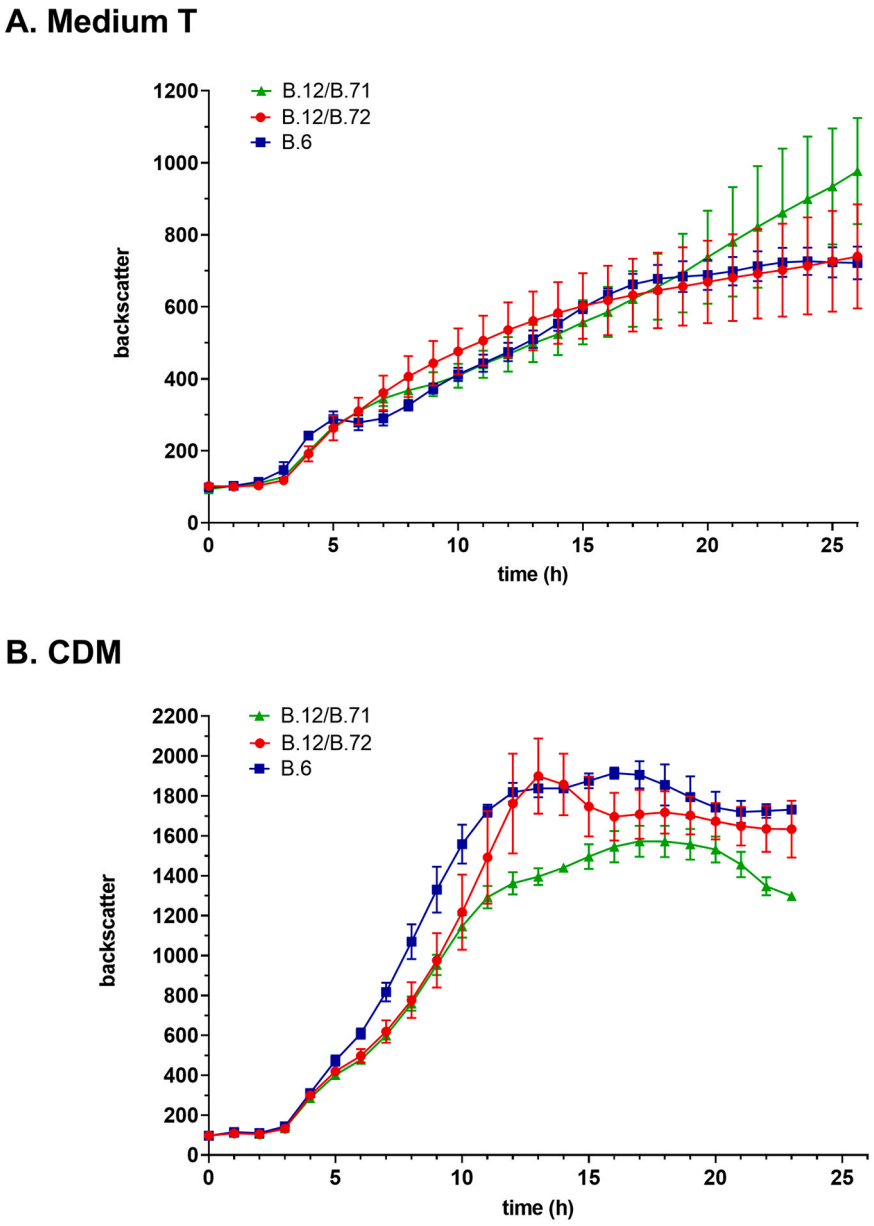

Fig. 3. Investigation of clade-specific growth behavior of *Fth* strains belonging to basal clade B.6 (in blue), clade B.71 (in green) and clade B.72 (in red) in medium T (A) and CDM (B). In contrast to Fig. 2, in this figure, results of three different strains of each clade were used and results are mean backscatter values with standard deviations of 10 independent experiments. Backscatter values were measured each hour, up to 26 h (medium T) or 23 h (CDM).

strains of B.6 are mainly found in southwestern regions, whereas strains of clade B.12 are more present in northeastern parts of the country (Appelt et al., 2019; Gyuranecz et al., 2012; Koene et al., 2019). As mentioned in the introduction, little information is available about phenotypical differences between the basal clades of *Fth*, except for glycerol fermentation and erythromycin resistance of basal clade B.16 and B.12, respectively (Karlsson et al., 2016; Kudelina and Olsufiev, 1980). However, basal clades B.6 and B.12 have been reported display differences in pathogenicity in lagomorphs (Hestvik et al., 2018; Kreizinger et al., 2017; Origgi et al., 2014; Origgi and Pilo, 2016). Isolates of clade B.6, for instance, seem more often involved in cases of tularemia patients showing symptoms of pneumonia (Appelt et al., 2019). Here, we introduce the analysis of a recently identified new clade (B.71) of *Fth* belonging to basal clade B.12. We demonstrate differences in the backscatter light intensity curves, as well as genomic and proteomic differences of the three *Fth* clades (B.6, B.71 and B.72) investigated in this study.

Fth isolates obtained from a human patient (2018), from a wild boar (2005) and from a racoon dog (2012) in Berlin and Brandenburg, Germany, were identified as members of the new clade B.71 of basal clade B.12 (Schulze et al., 2016). Recently, *Fth* strain 14T0224 isolated from *Lepus europaeus* (2014) in Schleswig-Holstein, Germany, was also identified as a member of clade B.71 (Linde et al., 2020). We could show that the new clade B.71 represents a sister clade to clade B.72 (Fig. 1). We demonstrated that B.71 and B.72 both represent clades within basal clade B.12, based on the results of phylogenetic analysis of the genome sequences (Fig. 1).

To generate a reference genome for clade B.71, *Fth* patient isolate A-1341 was chosen. We, consequently, generated and analyzed the complete genome of this strain. The genome is 1,893,440 bp in length with a GC content of 32.2%, which is in general agreement of strains of *Fth*. We identified various genomic differences of this new clade when comparing it to the other members (B.72) of basal clade B.12. Analysis revealed 245 B.71-specific SNPs and 24 Indels, again confirming B.71 to

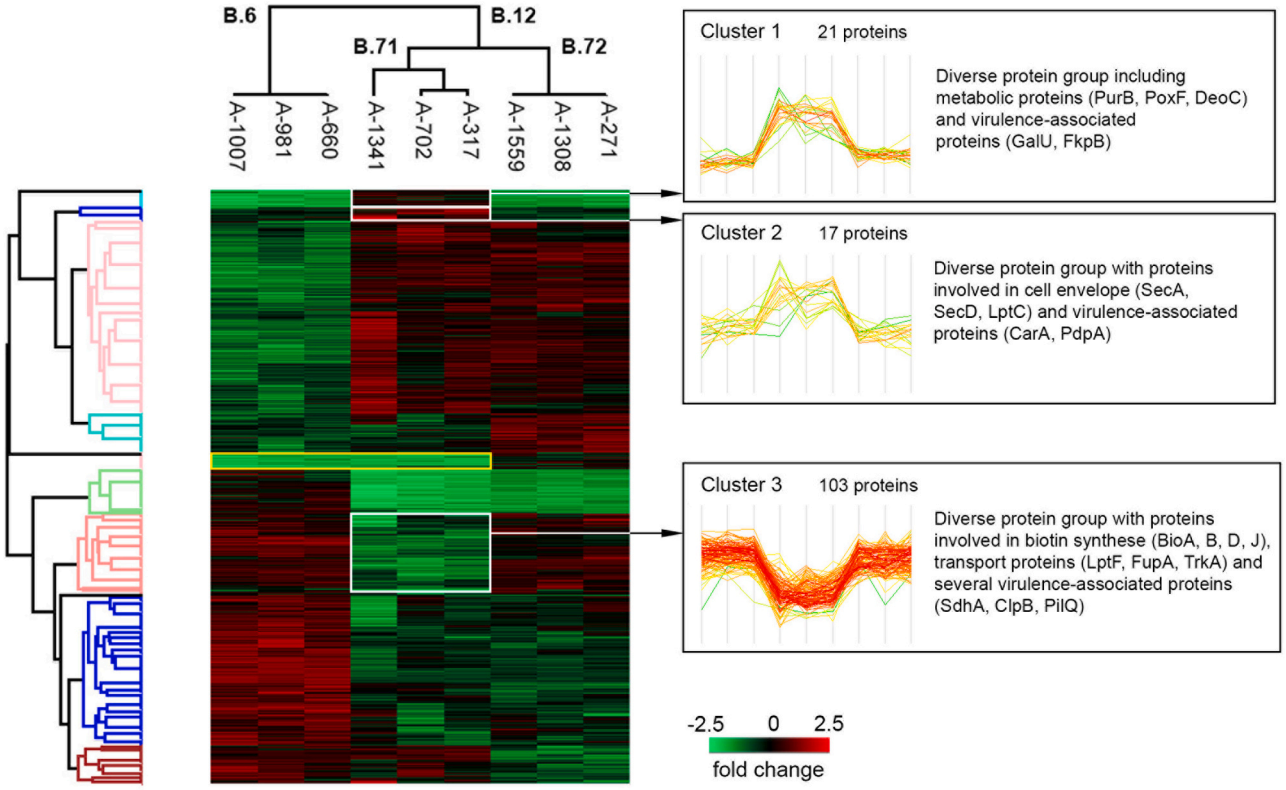

Fig. 4. Heat Map: *Fth* strain specific alteration in proteomes of three B.71, B.72 and B.6 strains, respectively. Bacteria were cultured on MTKH plates for 24 h. Samples were prepared using the SPEED method and analyzed using Perseus. The heatmap displays the altered abundance of 745 proteins of nine *Fth* wildtype strains (B.71: A-317, A-702, A-1341; B.72: A-271, A-1308, A-1559; B.6: A-660, A-981, A-1007) which were analyzed in three independent replicates. The proteins are represented by their average log2-transformed intensities using hierarchical clustering. Three main B.71-specific abundance clusters (white frames) were identified with 21, 17 and 103 proteins, respectively. The cluster profile plots and few selected proteins are depicted. The yellow frame highlights a protein abundance cluster which is more similar between B.71 and B.6 strains.

be an own and relatively distant related clade of B.12. This finding is also supported by the identification of seven B.72 clade-specific deletions, not present in strains of B.71. Furthermore, we identified a further B.71-specific canSNP in the highly conserved region of 16 s rDNA, in addition to the earlier identified B.71-specific canSNP (position 1,330,179, ancestral SNP state G/derived SNP state A in FSC200 reference genome [GenBank accession number CP003862.1]) (Schulze et al., 2016). Interestingly, for various genes inactivated (stop codon, frame-shift) in strains of B.71, we could identify a significantly lower amount of the corresponding proteins in the proteomes analyzed (e.g. DnaE, Asd), underpinning the findings at genome level and demonstrating the "robustness" of the LC-MS/MS method. It also emphasizes the importance of gaining complete genome sequences of at least one strain of each clade for further analysis of clade-specific geno- and phenotypes. Very recently it was shown that comparative LC-MS/MS analysis may also be used to distinguish antibiotic-resistant strains of *Francisella* from antibiotic-sensitive strains (Deatherage Kaiser et al., 2022).

We confirmed that B.71 and B.72 both represent distinct clades within basal clade B.12 by comparing the whole proteomes of strains of the different clades B6, B.71 and B.72 (Fig. 4). The results clearly indicate that members of clade B.71 exhibit a significantly different proteome pattern than strains of clade B.72, showing that phylogenetically different clades are recognizable by the expression pattern of the whole proteomes of the respective strains (for details, see below). The same applies to clade-specific phenotypic differences, as shown here in clade-specific growth behavior of the strains analyzed (Fig. 2 and Fig. 3). Observed differences in the pattern of proteins, involved in DNA replication and repair, in (carbohydrate) metabolism, protein biosynthesis and cell wall synthesis may explain the findings of the clade-specific differences of the growth curve of strains belonging to clade B.71 (Fig. 3). During growth in liquid media, strains belonging to clade B.71 revealed a common overall backscatter curve, which was different from strains belonging to clade B.72, as well as from strains of basal clade B.6. Thus, we demonstrated, for the first time, that the phylogenetic typing of (basal) clades can, indeed, be associated with characteristic phenotypes of the strains, in addition to the described erythromycin resistance of members of basal clade B.12 (Karlsson et al., 2016; Kudelina and Olsufiev, 1980; Tomaso et al., 2017).

We also investigated further putative phenotypes hypothesized due to the gene function of those genes that are differently expressed or inactivated (pseudogenes) within members of the investigated clades. As mentioned above, we identified clade-specific differences in the overall backscatter intensity curves. Comparing backscatter values with OD_{600} and CFU values, we are able to demonstrate that the backscatter method is suitable to investigate the growth of *Fth*, as shown previously for other microorganisms (Bruder et al., 2016; Hemmerich et al., 2017). It is known that backscattering intensities are influenced by morphological or cell size related deviations due to cell differentiation. Metabolic changes could also be involved in varying backscatter (scattered light intensity) values (Bruder et al., 2016; Latimer and Pyle, 1972). For example, backscatter values were shown to be able to indicate a diauxic shift, e.g. a second retarded growth in the case of growth on arising metabolites (Eiteman and Altman, 2006; Hemmerich et al., 2017). However, we can show here that the Cell Growth Quantifier can also be used for *Francisella* to analyze the general behavior (biomass, morphology and cell size) of strains in liquid media. Morphological differences during growth or proteins present in the cell envelope of strains of B.71, B.72 and B.6 might be involved in the clade-specific backscattering of light observed with the Cell Growth Quantifier (Tables 3 and 4). In addition, this method is particularly suitable for the

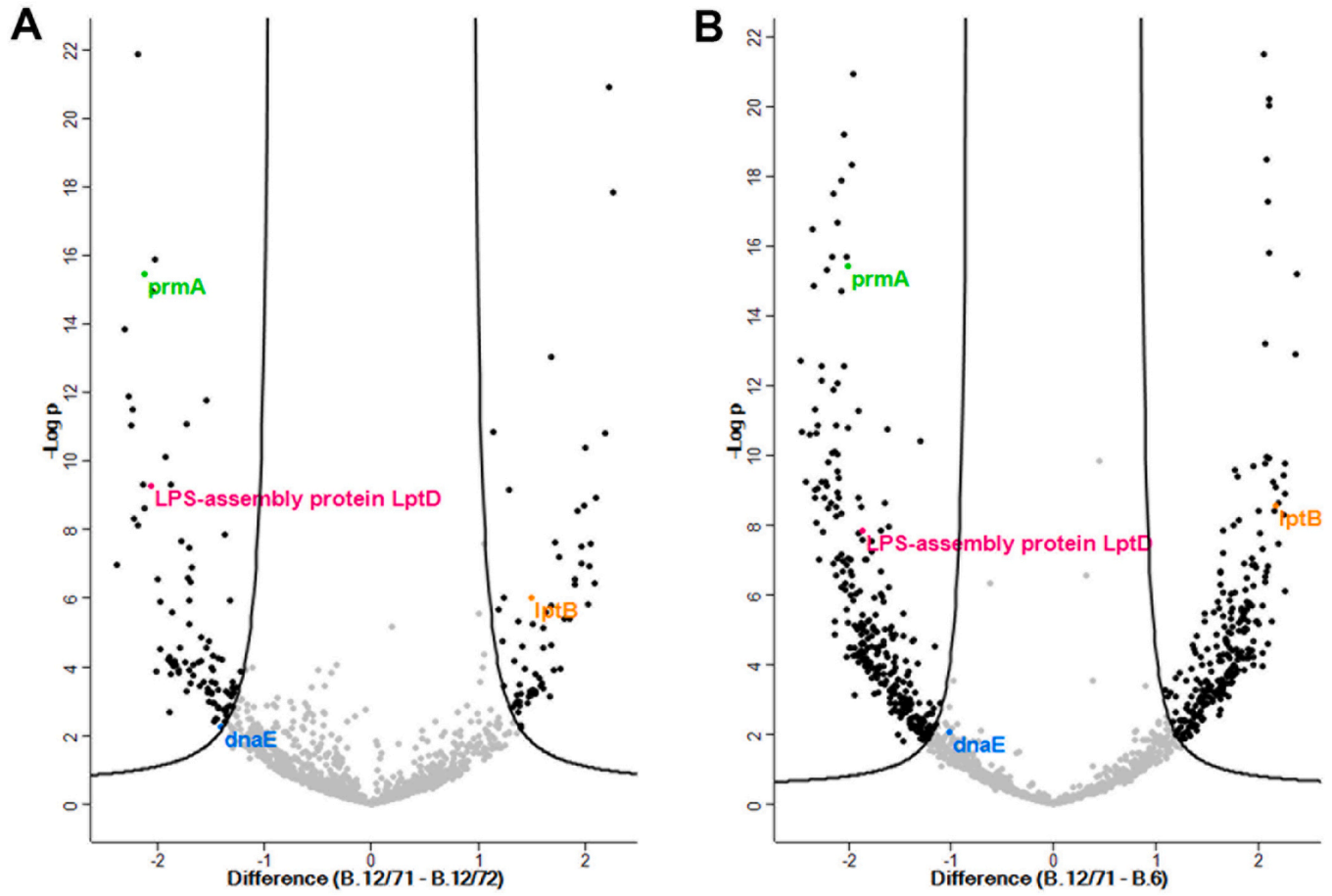

Fig. 5. Volcano Plot: Differential proteomes of *Fth* clades. Bacteria were cultured on MTKH plates for 24 h. Samples were prepared using the SPEED method and analyzed using Perseus. The proteome of *Fth* B.71 was compared to that of *Fth* B.72 (A) and *Fth* B.6 (B). Volcano line was generated using FDR = 0.01 and S0 = 1. The x-axis represents the fold change in logarithmic scale (difference), the y-axis the –log(pvalue) indicating the significant strength. Gene products (DnaE (blue), PmrA (green), LptD (pink)) with promotor regions, that possess deletions specific for B.71 strains, are highlighted. Possessing a specific SNP in B.71 without negatively affecting protein abundance, *lptB* has been marked orange.

determination of growth behavior (backscatter light intensity) of highly pathogenic bacteria, since the measurement is automatically effected without any need to open the flask during the experiment. Especially, when working with highly pathogenic microorganisms, as *Fth and Ftt,* this is an important safety aspect.

Generally, proteomic comparisons of subspecies are challenging, as minor peptide/protein sequence variants might show different quantification results when using conventional mass spectrometry analysis software platforms and corresponding quantification algorithms (Klimentova et al., 2021). To resolve this issue, we combined and analyzed three single-species databases using *Fth* FDC408 (A-271_1) as a reference of the B.72 clade, *Fth* A-1341 for B.71 and *Fth* FTNF002–00 for B.6. In total, 1349 homologues proteins were identified. In support of the genotypic analyses, we did not find any gene products of predicted pseudogenes (Table 1B) within the proteome of *Fth* A-1341. Also, PmrA and LptD were significantly lower expressed in B.71 confirming the deletions in its putative promotor regions (Table 1B, Fig. 5). As expected, strains belonging to clade B.71 possessed less differences in protein abundance with B.72 strains (167 proteins were significantly different) compared to B.6 strains (559 proteins were significantly different, Fig. 5). Our proteomic data showed that many proteins, which are higher expressed in B.71 compared to B.72 and B.6, are often metabolic/biosynthetic and ribosomal proteins (Table 3, Tab. S2). On the contrary, many proteins of the bacterial cell envelope/outer membrane/pilus, DNA replication and repair, as well as of proteins involved in the synthesis of biotin, pyridoxalphosphate and riboflavin (*ribD*) are lower expressed in B.71 compared to B.6 and B.72. Our data are consistent with the observation of Klimentova and colleagues (Klimentova et al., 2021), who detected different abundances of bacterial cell surface proteins (like PilF, FopA and MlaD) in outer membrane vesicles obtained from moderately virulent *Fth* and highly virulent *Ftt*. Also, Shibata and colleagues (Shibata et al., 2022) analyzed and compared the proteome of a highly pathogenic and predominant intracellular *Ftt* strain with a free-living and "non-virulent" *Fno* strain. Here, they found a significant upregulation of genes involved in biotin syntheses in *Ftt* compared to *Fno*. Interestingly, our proteomic data revealed a lower abundance of BioA, BioB, BioD and BioJ in B.71 strains compared to B.72 and B.6. Moreover, BioB, BioD and BioJ were significantly increased in B.6 compared to basal clade B.12 (=B.71 +B.72 strains). First, we found expression differences between *Fth* subspecies complementary to the species-specific differences identified by Shibata et al. (Shibata et al., 2022). BioJ has been proven essential for intracellular replication in macrophages and for full virulence in mice of *Fno* (Feng et al., 2014; Napier et al., 2012).

We identified putative virulence factors of *Francisella* which are inactivated (predicted pseudogene *malA*) in strains of B.71 and also showed differences in the protein amount of known virulence factors, such as glycine-cleavage system [glycine dehydrogenase], PPIase, gluconeogenesis [phospho-pyrovate dikinase, Fructose-bis phosphate phosphatase] pentose phosphate shunt [ribose-5-phosphate isomerase], glycerol catabolism, (Brissac et al., 2015; Brown et al., 2014; Chen et al., 2017; Radlinski et al., 2018; Rytter et al., 2021; Ziveri et al., 2017a;

Table 3
Selected proteins with higher abundance in B.71.

Gene	Locus tag NF101_[a]	B.71 vs. B.72		B.71 vs. B.6		B.12 vs. B.6[b]	Putative protein name	Biological process/molecular function[c]
		Signi.	Dif.	Signi.	Dif.			
alaS	05640[2]	+	1.97	+	2.25	+	Alanine–tRNA ligase	Protein biosynthesis
bamA	02770[2]	+	1.51	+	1.89	+	Outer membrane protein assembly factor	Cell adhesion
carA	00155[2]	+	1.48	+	1.64		Carbamoyl-phosphate synthase small chain	Amino-acid biosynthesis, Antibiotic biosynthesis[#]
carB	00150	+	1.28	+	2.36	+	Carboxymethylproline synthase	Antibiotic biosynthesis[#]
deoC	08435[1]	+	1.66		0.83		2-deoxy-D-ribose 5-phosphate aldolase	Lyase
fkpB	01665[1]	+	1.38		1.03		Peptidyl-prolyl cis-trans isomerase	Protein folding
galU	06925[1]	+	1.90	+	1.73		UTP–glucose-1-phosphate uridylyltransferase	Stationary phase survival[#]
glgA	02500	+	2.22		0.32		Glycogen synthase	Glycogen biosynthesis/metabolism
glgC	02495	+	2.26		0.44		Glucose-1-phosphate adenylyltransferase	Glycogen biosynthesis/metabolism
lptB	05450	+	1.50	+	2.16	+	Lipopolysaccharide export system ATP-binding protein	Transport
lptC	05440	+	1.60	+	1.95	+	Lipopolysaccharide export system protein	Transport
malQ	02510	+	1.32	+	1.49		4-alpha-glucanotransferase	Carbohydrate metabolism
mutS	01500[1]	+	1.56	+	1.48		DNA mismatch repair protein MutS	DNA damage, repair
panG	03490[2]	+	1.60	+	1.90	+	2-dehydropantoate 2-reductase	Oxireductase
pdpA	00605[2]	+	1.59	+	1.89	+	pathogenicity determinant protein PdpA1	Type VI secretion system[#]
purB	09375[1]	+	1.72	+	2.14	+	Adenylosuccinase	Purine biosynthesis
pyrB	00145	+	1.14	+	2.38	+	Aspartate carbamoyltransferase catalytic subunit	Pyrimidine biosynthesis[#]
recB	03460	+	1.24		-0.74		RecBCD enzyme subunit RecB	DNA damage/repair[#]
recN	01960	+	1.38	+	1.74		DNA repair protein RecN	DNA damage/repair
secA	07450[2]	+	1.76	+	2.04	+	Protein translocase subunit SecA	Transport
secD	04365[2]	+	1.53	+	1.79		Protein translocase subunit SecD	Transport
	06660[1]	+	1.93	+	2.01		ferredoxin–NADP reductase	Secondary metabolite biosynthesis[#]
aroA	04385		-0.14	+	1.68	+	3-phosphoshikimate 1-carboxyvinyltransferase	Amino-acid biosynthesis[#]
aroQ	08085[1]		0.74	+	1.31		3-dehydroquinate dehydratase	Amino-acid biosynthesis
coaBC	04170		0.38	+	1.50	+	Coenzyme A biosynthesis bifunctional protein CoaBC	Multifunctional enzyme, coenzyme A biosynthesis
coaD	06780		0.36	+	1.61	+	Phosphopantetheine adenylyltransferase	Coenzyme A biosynthesis
coaE	01585		-0.03	+	1.48	+	Dephospho-CoA kinase	Coenzyme A biosynthesis
fabF	05810		0.02	+	1.94	+	3-oxoacyl-[acyl-carrier-protein] synthase 2	Fatty acid biosynthesis/metabolism
fabZ	02785		-0.26	+	1.65	+	3-hydroxyacyl-[acyl-carrier-protein] dehydratase	Lipid A biosynthesis[#]
feoB	00660		-0.54	+	1.65	+	Fe(2 +) transporter FeoB	Iron transport[#]
galE	07330		0.67	+	1.56	+	UDP-glucose 4-epimerase	Carbohydrate metabolism[#]
glpK	08345		0.08	+	2.11	+	Glycerol kinase	Glycerol metabolism
glpX	08610		0.05	+	2.09	+	Fructose-1,6-bisphosphatase class 2	Carbohydrate metabolism[#]
hemC	00695		-0.54	+	1.44	+	Porphobilinogen deaminase	Porphyrin biosynthesis
hemE	09205		-0.28	+	1.36	+	Uroporphyrinogen decarboxylase	Porphyrin biosynthesis
lptE	06200		-0.59	+	1.69	+	LPS-assembly lipoprotein	Transport[#]
lpxC	09650		-0.45	+	1.20	+	UDP-3-O-acyl-N-acetylglucosamine deacetylase	Lipid A biosynthesis[#]
murQ	01525		0.95	+	1.87	+	N-acetylmuramic acid 6-phosphate etherase	Carbohydrate metabolism
mutM	07850		0.48	+	1.85	+	Formamidopyrimidine-DNA glycosylase	DNA damage/repair
panB	03485		0.00	+	2.07	+	3-methyl-2-oxobutanoate hydroxymethyltransferase	Pantothenate biosynthesis
panC	03480		0.05	+	2.10	+	Pantothenate synthetase	Pantothenate biosynthesis
pheS	06140		0.75	+	1.73	+	Phenylalanine–tRNA ligase alpha subunit	Protein biosynthesis
pheT	06145		0.01	+	1.57	+	Phenylalanine–tRNA ligase beta subunit	Protein biosynthesis
ppdK	00655		0.26	+	1.93	+	Pyruvate, phosphate dikinase	Transferase, ATP-binding[#]
purL	09420		0.20	+	1.70	+	Phosphoribosylformylglycinamidine synthase subunit	Purine biosynthesis
rbfA	09180		0.51	+	1.44	+	30 S ribosome-binding factor	Ribosome biosynthesis, stress response
rplA *	08860		0.37	+	1.87	+	50 S ribosomal protein L1	Ribosomal protein
rpmC	01240		0.43	+	1.82	+	50 S ribosomal protein L29	Ribosomal protein
rpmD	01290		0.20	+	1.38	+	50 S ribosomal protein L30	Ribosomal protein
rpoC	08840		0.02	+	1.51	+	DNA-directed RNA polymerase subunit beta	Antibiotic resistance, transcription
rpoD	05380		0.21	+	1.88	+	RNA polymerase sigma factor RpoD	Transcription, transcription regulation[#]
rpsA°	09680		-0.23	+	1.54	+	30 S ribosomal protein S1	Ribosomal protein
tolQ	01690		0.26	+	1.90	+	Tol-Pal system protein TolQ	Cell division, cell cycle[#]
uvrA	07500		0.33	+	1.64	+	UvrABC system protein A	DNA damage, excision, repair, response
	05750		-0.06	+	1.44	+	Type II toxin-antitoxin system HipA family toxin	Toxin-antitoxin system[#]

Signi. = significant
Dif. = difference
[a] locus tags refer to strain *Fth* A-1341
[b] significant higher abundance in B.12 compared to B.6
[c] according to uniprot data base
[1] also found in cluster 1 in heatmap, see Fig. 4
[2] also found in cluster 2 in heatmap, see Fig. 4
* also rplB,C, D, F, I, J, K, M, N, O, P, Q, S, T, U, V, W, X significant higher abundance in B.71 compared to B.6, see supplement
° also rpsC, D, E, F, G, H, J, M, P, Q significant higher abundance in B.71 compared to B.6, see supplement
[#] associated with bacterial virulence

Table 4
Selected proteins with lower abundance in B.71.

Gene	Locus tag NF101_[a]	B.71 vs. B.72		B.71 vs. B.6		B.12 vs. B.6[b]	Putative protein name	Biological process/molecular function[c]
		Signi.	Dif.	Signi.	Dif.			
argS	08110[3]	+	-1.77	+	-2.15	+	Arginine–tRNA ligase	Protein biosynthesis
bioA	06510[3]	+	-2.05	+	-2.07		Adenosylmethionine-8-amino-7-oxononanoate aminotransferase	Biotin biosynthesis[#]
bioB	06515[3]	+	-1.68	+	-2.13	+	Biotin synthase	Biotin biosynthesis[#]
bioD	06530[3]	+	-1.51	+	-2.03	+	ATP-dependent dethiobiotin synthetase BioD 1	Biotin biosynthesis[#]
bioJ	06495[3]	+	-1.72	+	-2.26	+	Pimeloyl-ACP methyl ester esterase BioJ (BioH)	Biotin biosynthesis[#]
clpB	00460[3]	+	-2.02	+	-2.12	+	Chaperone protein ClpB	Chaperone, stress response[#]
dnaE	02425[3]	+	-1.41		-1.02		DNA polymerase III subunit alpha	DNA replication
fabD	05825[3]	+	-1.70	+	-1.55		Malonyl CoA-acyl carrier protein transacylase	Lipid metabolism[#]
fabG	05820[3]	+	-1.52		-0.43		3-oxoacyl-[acyl-carrier-protein] reductase	Lipid metabolism
gatA	09350	+	-1.26		0.54		PTS system galactitol-specific EIIA component	Phosphotransferase system, sugar transport
gatB	09345	+	-2.00		-0.69		PTS system galactitol-specific EIIB component	Phosphotransferase system, sugar transport
gyrB	07870[3]	+	-1.67		-0.49		DNA gyrase subunit B	DNA replication
ilvC	04680[3]	+	-2.18	+	-1.96		Ketol-acid reductoisomerase (NADP(+))	Amino-acid biosynthesis
lptD	08105[3]	+	-2.06	+	-1.87		LPS-assembly protein	Outer membrane assembly[#]
mnmE	06040[3]	+	-1.37	+	-1.31		tRNA modification GTPase	tRNA processing[#]
nuoG	09265[3]	+	-1.71	+	-2.10	+	NADH-quinone oxidoreductase subunit G[#]	Respiratory electron transport chain[#]
pilB	04265	+	-1.49		-0.86		Type IV pilus assembly ATPase	Pilus[#]
pilQ	04125	+	-1.43	+	-1.63		Type IV pilus secretin PilQ family protein	Pilus[#]
prmA	04980	+	-2.12	+	-2.01		Ribosomal protein L11 methyltransferase	Ribosomal protein, transferase
ruvC	04745	+	-2.14		-0.34		Crossover junction endodeoxyribonuclease	DNA damage/recombination/ repair[#]
sdhA	09070[3]	+	-1.43	+	-1.30		Succinate dehydrogenase flavoprotein subunit	Electron transport, Tricarboxylic acid cycle[#]
serC	05200[3]	+	-1.35	+	-1.34		Phosphoserine aminotransferase	Amino-acid biosynthesis[#]
uvrB	03850[3]	+	-1.53		-0.59		UvrABC system protein B	DNA damage/excision/repair, SOS response[#]
	05340[3]	+	-1.70	+	-2.13	+	FKBP-type peptidyl-prolyl cis-trans isomerase	
	02220[3]	+	-1.86	+	-1.75		DUF3573 domain-containing protein	
	04105[3]	+	-1.29	+	-1.85	+	Type IV pili	Pilus[#]
asd	02315[3]		-0.83	+	-1.51	+	Aspartate-semialdehyde dehydrogenase	Amino-acid biosynthesis
clpP	04575		-0.42	+	-1.49		ATP-dependent Clp protease proteolytic subunit	Chaperone, stress response[#]
dusA	07880		-0.29	+	-1.74	+	tRNA-dihydrouridine(20/20a) synthase	tRNA processing
fopA	06770		0.19	+	-1.20	+	Outer membrane protein A	Outer membrane protein[#]
groL	08680		0.41	+	-1.69	+	Chaperonin GroEL	Chaperone[#]
hfq	04605		-1.04	+	-1.57		RNA-binding protein Hfq	Stress response[#]
katG	07660		0.48	+	-1.69	+	Catalase-peroxidase	Hydrogen peroxide, metal-bining[#]
kdsA	07810[3]		-1.12	+	-1.70	+	2-dehydro-3-deoxyphosphooctonate aldolase	Lipopolysaccharide biosynthesis
lpxB	02795		-0.25	+	-1.77	+	Lipid-A-disaccharide synthase	Lipid A biosynthesis
lpxD	02780		0.22	+	-1.42	+	UDP-3-O-acylglucosamine N-acyltransferase	Lipid A biosynthesis[#]
minC	02675		0.05	+	-1.84	+	Septum site-determining protein	Cell division[#]
minD	02670		-0.01	+	-1.69	+	Septum site-determining protein	Cell division[#]
mnmC	03940		-0.40	+	-1.63	+	tRNA 5-methylaminomethyl-2-thiouridine biosynthesis bifunctional protein	tRNA processing
murD	08195[3]		-1.10	+	-1.38		UDP-N-acetylmuramoylalanine–D-glutamate ligase	Cell wall biogenesis/degradation
nuoF	09270		-0.41	+	-1.54	+	NADH-quinone oxidoreductase subunit F	Translocase
parC	02375		0.31	+	-1.57	+	DNA topoisomerase 4 subunit A	DNA-binding, isomerase
parE	08750		-1.10	+	-1.70	+	DNA topoisomerase 4 subunit B	DNA-binding, isomerase, antibiotic resistance
pdxS	07865		-0.32	+	-2.21	+	Pyridoxal 5′-phosphate synthase subunit PdxS	Lyase[#]
pdxT	07860		-0.23	+	-2.16	+	Pyridoxal 5′-phosphate synthase subunit PdxT	Lyase[#]
pdxY	01005		-0.74	+	-1.55	+	Pyridoxal kinase	ATP-binding, kinase
pilO	04115		-0.97	+	-1.89	+	Type 4a pilus biogenesis protein	Pilus[#]
ppk2	02820		0.04	+	-1.88	+	Protein kinase domain-containing protein ppk2	ATP-binding, protein phosphorylation
recC	03445		-1.00	+	-1.60	+	RecBCD enzyme subunit RecC	DNA damage/repair/ recombination[#]
recD	03465		0.16	+	-1.78	+	RecBCD enzyme subunit RecD	DNA damage/repair[#]
recG	02695		-0.36	+	-1.26		ATP-dependent DNA helicase RecG	DNA damage/repair/recombination
recJ	08040[3]		-0.98	+	-1.55		Single-stranded-DNA-specific exonuclease RecJ	DNA-binding, exonuclease
recR	07215		-0.77	+	-1.43		Recombination protein RecR	DNA damage/repair/recombination
ribD	00385		0.05	+	-1.90	+	Riboflavin biosynthesis protein	Riboflavin biosynthesis
	04110[3]		-1.12	+	-1.85	+	PilN domain-containing protein	Pilus[#]
	00915		-0.72	+	-1.53	+	Type IV pilin protein	Pilus[#]
	03595		-0.65	+	-1.60	+	MlaD family protein	Transport[#]
	03930[3]		-0.78	+	-1.19		Type II toxin-antitoxin system RatA family toxin	Toxin-antitoxin system[#]

Signi. = significant
Dif. = difference
[a] locus tags refer to strain *Fth* A-1341
[b] significant higher abundance in B.12 compared to B.6
[c] according to uniprot data base

[3] also found in cluster 3 in heatmap, see Fig. 4
[#] associated with bacterial virulence

Ziveri et al., 2017b), *bio* operon (biotin synthesis), *dinB*, riboflavin biosynthesis (*ribB*) (Mehta et al., 2022; Napier et al., 2012; Shibata et al., 2022). Until now, we do not know if these expression differences have an impact on bacterial fitness or virulence. This still needs to be clarified.

We showed that the hierarchical clustering based on the proteomic expression profile of nine *Fth* strains reflects the canSNP analyses and the phylogenetic clustering based on mauve alignment and neighbor joining bootstrap clustering of nearly whole genome sequences (Fig. 1 and Fig. 4). Here, *Fth* strains A-660, A-981 and A-1007, forming basal clade B.6, are separated from basal clade B.12 strains which are divided into two distinct clades: B.71 (A-317, A-702 and A-1341) and B.72 (A-271, A-1308, A-1559; Fig. 4). The proteomic profiles of 745 proteins in nine *Fth* strains revealed three B.71-specific protein expression clusters: two consist of significantly higher expressed proteins (in total 37 proteins), whereas the third, with 103 proteins, consists of lower expressed proteins in B.71 strains. Interestingly, some proteins of B.71 strains showed more similar expression levels obtained for B.6 strains than for B.72 strains, substantiating the unique position of B.71 strains also sharing common SNPs with B.6.

5. Conclusion

In general, a growth rate-based analysis, employing different growth regimes, can be used to characterize mutant strains or strains with chromosomal modifications as these have diverse impact on the fitness of the bacterium (Hemmerich et al., 2017; Unthan et al., 2015). Thus, our results indicate that there may be differences in the fitness of *Fth* strains belonging to the different clades. As previously published, B.12 and B.6 clades may display differences in pathogenicity (Appelt et al., 2019; Hestvik et al., 2018; Koene et al., 2019; Kreizinger et al., 2017; Origgi et al., 2014). Further experimental data is needed to confirm reports about differences in virulence between strains of basal clades B.12 and B.6.

Fth isolates can be distinguished by phylogenetic tree analysis (genome based) and, as recently published, it even seems possible to discriminate *Fth* strains of basal clades B.12 and B.6 by proteomic profiling using mass spectrometry (Witt et al., 2020). In this study, we could corroborate these findings also for strains of the new clades B.71 and B.72 of clade B.12, and could demonstrate that this differentiation also seems to correlate with the backscatter light intensity curves of the respective isolates. It will be interesting to further analyse, if differences in pathogenicity or fitness exist between the members of the different clades. Experiments are under way to investigate these interesting questions.

Declaration of Competing Interest

All authors declare no conflict of interest.

Acknowledgments

This work was supported by the Robert Koch Institute.

Appendix A. Supporting information

Supplementary data associated with this article can be found in the online version at doi:10.1016/j.ijmm.2023.151583.

References

Abdellahoum, Z., Maurin, M., Bitam, I., 2020. Tularemia as a mosquito-borne disease. Microorganisms 9.
Appelt, S., Faber, M., Koppen, K., Jacob, D., Grunow, R., Heuner, K., 2020. Francisella tularensis subspecies holarctica and tularemia in Germany. Microorganisms 8.
Appelt, S., Koppen, K., Radonic, A., Drechsel, O., Jacob, D., Grunow, R., Heuner, K., 2019. Genetic diversity and spatial segregation of francisella tularensis subspecies holarctica in Germany. Front Cell Infect. Microbiol 9, 376.
Becker, S., Lochau, P., Jacob, D., Heuner, K., Grunow, R., 2016. Successful re-evaluation of broth medium T for growth of Francisella tularensis ssp. and other highly pathogenic bacteria. J. Microbiol Methods 121, 5–7.
Beckstrom-Sternberg, S.M., Auerbach, R.K., Godbole, S., Pearson, J.V., Beckstrom-Sternberg, J.S., Deng, Z., Munk, C., Kubota, K., Zhou, Y., Bruce, D., Noronha, J., Scheuermann, R.H., Wang, A., Wei, X., Wang, J., Hao, J., Wagner, D.M., Brettin, T.S., Brown, N., Gilna, P., Keim, P.S., 2007. Complete genomic characterization of a pathogenic A.II strain of Francisella tularensis subspecies tularensis. PLoS One 2, e947.
Bolger, A.M., Lohse, M., Usadel, B., 2014. Trimmomatic: a flexible trimmer for Illumina sequence data. Bioinformatics 30, 2114–2120.
Brissac, T., Ziveri, J., Ramond, E., Tros, F., Kock, S., Dupuis, M., Brillet, M., Barel, M., Peyriga, L., Cahoreau, E., Charbit, A., 2015. Gluconeogenesis, an essential metabolic pathway for pathogenic Francisella. Mol. Microbiol 98, 518–534.
Brown, M.J., Russo, B.C., O'Dee, D.M., Schmitt, D.M., Nau, G.J., 2014. The contribution of the glycine cleavage system to the pathogenesis of Francisella tularensis. Microbes Infect. 16, 300–309.
Bruder, S., Reifenrath, M., Thomik, T., Boles, E., Herzog, K., 2016. Parallelised online biomass monitoring in shake flasks enables efficient strain and carbon source dependent growth characterisation of Saccharomyces cerevisiae. Micro Cell Fact. 15, 127.
Burckhardt, F., Hoffmann, D., Jahn, K., Heuner, K., Jacob, D., Vogt, M., Bent, S., Grunow, R., Zanger, P., 2018. Oropharyngeal tularemia from freshly pressed grape must. N. Engl. J. Med 379, 197–199.
Challacombe, J.F., Petersen, J.M., Gallegos-Graves, L.V., Hodge, D., Pillai, S., Kuske, C. R., 2017. Whole-genome relationship among francisella bacteria of diverse origins define new species and provide specific regions for detection. Appl. Environ. Microbiol 83, e02589–16.
Chamberlain, R.E., 1965. Evaluation of live tularemia vaccine prepared in a chemically defined medium. Appl. Microbiol 13, 232–235.
Champion, M.D., Zeng, Q., Nix, E.B., Nano, F.E., Keim, P., Kodira, C.D., Borowsky, M., Young, S., Koehrsen, M., Engels, R., Pearson, M., Howarth, C., Larson, L., White, J., Alvarado, L., Forsman, M., Bearden, S.W., Sjostedt, A., Titball, R., Michell, S.L., Birren, B., Galagan, J., 2009. Comparative genomic characterization of Francisella tularensis strains belonging to low and high virulence subspecies. PLoS Pathog. 5, e1000459.
Chen, F., Rydzewski, K., Kutzner, E., Hauslein, I., Schunder, E., Wang, X., Meighen-Berger, K., Grunow, R., Eisenreich, W., Heuner, K., 2017. Differential Substrate Usage and Metabolic Fluxes in Francisella tularensis Subspecies holarctica and Francisella novicida. Front Cell Infect. Microbiol 7, 275.
Clemens, D.L., Lee, B.Y., Horwitz, M.A., 2005. Francisella tularensis enters macrophages via a novel process involving pseudopod loops. Infect. Immun. 73, 5892–5902.
Deatherage Kaiser, B.L., Birdsell, D.N., Hutchison, J.R., Thelaus, J., Jenson, S.C., Andrianaivoarimanana, V., Bystrom, M., Myrtennas, K., McDonough, R.F., Nottingham, R.D., Sahl, J.W., Schweizer, H.P., Rajerison, M., Forsman, M., Wunschel, D.S., Wagner, D.M., 2022. Proteomic signatures of antimicrobial resistance in yersinia pestis and francisella tularensis. Front Med (Lausanne) 9, 821071.
Demichev, V., Messner, C.B., Vernardis, S.I., Lilley, K.S., Ralser, M., 2020. DIA-NN: neural networks and interference correction enable deep proteome coverage in high throughput. Nat. Methods 17, 41–44.
Doellinger, J., Schneider, A., Hoeller, M., Lasch, P., 2020. Sample preparation by easy extraction and digestion (SPEED) - A universal, rapid, and detergent-free protocol for proteomics based on acid extraction. Mol. Cell Proteom. 19, 209–222.
Dwibedi, C., Birdsell, D., Larkeryd, A., Myrtennas, K., Ohrman, C., Nilsson, E., Karlsson, E., Hochhalter, C., Rivera, A., Maltinsky, S., Bayer, B., Keim, P., Scholz, H. C., Tomaso, H., Wittwer, M., Beuret, C., Schuerch, N., Pilo, P., Hernandez Perez, M., Rodriguez-Lazaro, D., Escudero, R., Anda, P., Forsman, M., Wagner, D.M., Larsson, P., Johansson, A., 2016. Long-range dispersal moved Francisella tularensis into Western Europe from the East. Micro Genom. 2, e000100.
Edgar, R.C., 2004. MUSCLE: multiple sequence alignment with high accuracy and high throughput. Nucleic Acids Res 32, 1792–1797.
Eiteman, M.A., Altman, E., 2006. Overcoming acetate in Escherichia coli recombinant protein fermentations. Trends Biotechnol. 24, 530–536.
Ellis, J., Oyston, P.C., Green, M., Titball, R.W., 2002. Tularemia. Clin. Microbiol Rev. 15, 631–646.
Faber, M., Heuner, K., Jacob, D., Grunow, R., 2018. Tularemia in Germany-a Re-emerging Zoonosis. Front Cell Infect. Microbiol 8, 40.
Farlow, J., Wagner, D.M., Dukerich, M., Stanley, M., Chu, M., Kubota, K., Petersen, J., Keim, P., 2005. Francisella tularensis in the United States. Emerg. Infect. Dis. 11, 1835–1841.
Feng, Y., Napier, B.A., Manandhar, M., Henke, S.K., Weiss, D.S., Cronan, J.E., 2014. A Francisella virulence factor catalyses an essential reaction of biotin synthesis. Mol. Microbiol 91, 300–314.
Gyuranecz, M., Birdsell, D.N., Splettstoesser, W., Seibold, E., Beckstrom-Sternberg, S.M., Makrai, L., Fodor, L., Fabbi, M., Vicari, N., Johansson, A., Busch, J.D., Vogler, A.J., Keim, P., Wagner, D.M., 2012. Phylogeography of Francisella tularensis subsp. holarctica, Europe. Emerg. Infect. Dis. 18, 290–293.

Hemmerich, J., Wiechert, W., Oldiges, M., 2017. Automated growth rate determination in high-throughput microbioreactor systems. BMC Res Notes 10, 617.
Hestvik, G., Uhlhorn, H., Mattsson, R., Westergren, E., Sodersten, F., Akerstrom, S., Gavier-Widen, D., 2018. Pathology of natural Francisella tularensis subsp. holarctica infection in two yellow-necked mice (Apodemus flavicollis). Acta Vet. Scand. 60, 26.
Jacob, D., Koppen, K., Radonic, A., Haldemann, B., Zanger, P., Heuner, K., Grunow, R., 2019. Molecular identification of the source of an uncommon tularaemia outbreak, Germany, autumn 2016. Eur. Surveill. 24.
Johansson, A., Petersen, J.M., 2010. Genotyping of Francisella tularensis, the causative agent of tularemia. J. AOAC Int 93, 1930–1943.
Karlsson, E., Golovliov, I., Larkeryd, A., Granberg, M., Larsson, E., Ohrman, C., Niemcewicz, M., Birdsell, D., Wagner, D.M., Forsman, M., Johansson, A., 2016. Clonality of erythromycin resistance in Francisella tularensis. J. Antimicrob. Chemother. 71, 2815–2823.
Karlsson, E., Svensson, K., Lindgren, P., Bystrom, M., Sjodin, A., Forsman, M., Johansson, A., 2013. The phylogeographic pattern of Francisella tularensis in Sweden indicates a Scandinavian origin of Eurosiberian tularaemia. Environ. Microbiol 15, 634–645.
Kearse, M., Moir, R., Wilson, A., Stones-Havas, S., Cheung, M., Sturrock, S., Buxton, S., Cooper, A., Markowitz, S., Duran, C., Thierer, T., Ashton, B., Meintjes, P., Drummond, A., 2012. Geneious Basic: an integrated and extendable desktop software platform for the organization and analysis of sequence data. Bioinformatics 28, 1647–1649.
Keim, P., Johansson, A., Wagner, D.M., 2007. Molecular epidemiology, evolution, and ecology of Francisella. Ann. N. Y Acad. Sci. 1105, 30–66.
Kensy, F., Engelbrecht, C., Buchs, J., 2009. Scale-up from microtiter plate to laboratory fermenter: evaluation by online monitoring techniques of growth and protein expression in Escherichia coli and Hansenula polymorpha fermentations. Micro Cell Fact. 8, 68.
Kevin, M., Girault, G., Caspar, Y., Cherfa, M.A., Mendy, C., Tomaso, H., Gavier-Widen, D., Escudero, R., Maurin, M., Durand, B., Ponsart, C., Madani, N., 2020. Phylogeography and Genetic Diversity of Francisella tularensis subsp. holarctica in France (1947-2018). Front Microbiol 11, 287.
Klimentova, J., Rehulka, P., Pavkova, I., Kubelkova, K., Bavlovic, J., Stulik, J., 2021. Cross-species proteomic comparison of outer membrane vesicles and membranes of francisella tularensis subsp. tularensis versus subsp. holarctica. J. Proteome Res 20, 1716–1732.
Koene, M., Rijks, J., Maas, M., Ruuls, R., Engelsma, M., van Tulden, P., Kik, M., J, I.J., Notermans, D., de Vries, M., Fanoy, E., Pijnacker, R., Spierenburg, M., Bavelaar, H., Berkhout, H., Sankatsing, S., Diepersloot, R., Myrtennas, K., Granberg, M., Forsman, M., Roest, H.J., Grone, A., 2019. Phylogeographic distribution of human and hare francisella tularensis subsp. holarctica strains in the Netherlands and Its Pathology in European Brown Hares (Lepus europaeus). Front Cell Infect. Microbiol 9, 11.
Kreizinger, Z., Erdelyi, K., Felde, O., Fabbi, M., Sulyok, K.M., Magyar, T., Gyuranecz, M., 2017. Comparison of virulence of Francisella tularensis ssp. holarctica genotypes B.12 and B.FTNF002-00. BMC Vet. Res 13, 46.
Kudelina, R.I., Olsufiev, N.G., 1980. Sensitivity to macrolide antibiotics and lincomycin in Francisella tularensis holarctica. J. Hyg. Epidemiol. Microbiol Immunol. 24, 84–91.
Latimer, P., Pyle, B.E., 1972. Light scattering at various angles. Theoretical predictions of the effects of particle volume changes. Biophys. J. 12, 764–773.
Linde, J., Homeier-Bachmann, T., Dangel, A., Riehm, J.M., Sundell, D., Ohrman, C., Forsman, M., Tomaso, H., 2020. Genotyping of Francisella tularensis subsp. holarctica from Hares in Germany. Microorganisms 8.
Maurin, M., Gyuranecz, M., 2016. Tularaemia: clinical aspects in Europe. Lancet Infect. Dis. 16, 113–124.
Mehta, H.H., Ibarra, D., Marx, C.J., Miller, C.R., Shamoo, Y., 2022. Mutational switchbacks can accelerate evolution of francisella to a combination of ciprofloxacin and doxycycline. Front Microbiol 13, 904822.
Mihelcic, M., Marecic, V., Ozanic, M., Kelava, I., Knezevic, M., Santic, M., 2020. Epidemiologic and epizootic data of tularemia in the past and in the recent history in Croatia. Microorganisms 8.
Myrtennas, K., Escudero, R., Zaballos, A., Gonzalez-Martin-Nino, R., Gyuranecz, M., Johansson, A., 2020. Genetic traces of the francisella tularensis colonization of Spain, 1998-2020. Microorganisms 8.
Napier, B.A., Meyer, L., Bina, J.E., Miller, M.A., Sjostedt, A., Weiss, D.S., 2012. Link between intraphagosomal biotin and rapid phagosomal escape in Francisella. Proc. Natl. Acad. Sci. USA 109, 18084–18089.
Nelson, C.A., Murua, C., Jones, J.M., Mohler, K., Zhang, Y., Wiggins, L., Kwit, N.A., Respicio-Kingry, L., Kingry, L.C., Petersen, J.M., Brown, J., Aslam, S., Krafft, M., Asad, S., Dagher, H.N., Ham, J., Medina-Garcia, L.H., Burns, K., Kelley, W.E., Hinckley, A.F., Annambhotla, P., Carifo, K., Gonzalez, A., Helsel, E., Iser, J., Johnson, M., Fritz, C.L., Basavaraju, S.V., Tularemia in Transplant Recipients Investigation, T., 2019. Francisella tularensis transmission by solid organ transplantation, 2017(1). Emerg. Infect. Dis. 25, 767–775.
Öhrman, C., Sahl, J.W., Sjödin, A., Uneklint, I., Ballard, R., Karlsson, L., McDonough, R. F., Sundell, D., Soria, K., Bäckman, S., Chase, K., Brindefalk, B., Sozhamannan, S., Vallesi, A., Hägglund, E., Ramirez-Paredes, J.G., Thelaus, J., Colquhoun, D., Myrtennäs, K., Birdsell, D., Johansson, A., Wagner, D.M., Forsman, M., 2021. Reorganized genomic taxonomy of francisellaceae enables design of robust environmental PCR assays for detection of Francisella tularensis. Appl. Environ. Microbiol. 2017 83, e00174–17.
Origgi, F.C., Frey, J., Pilo, P., 2014. Characterisation of a new group of Francisella tularensis subsp. holarctica in Switzerland with altered antimicrobial susceptibilities, 1996 to 2013. Eur. Surveill. 19.
Origgi, F.C., Pilo, P., 2016. Francisella Tularensis Clades B.FTN002-00 and B.13 are associated with distinct pathology in the European brown hare (Lepus europaeus). Vet. Pathol. 53, 1220–1232.
Oyston, P.C., Griffiths, R., 2009. Francisella virulence: significant advances, ongoing challenges and unmet needs. Expert Rev. Vaccin. 8, 1575–1585.
Pavlovich, N.V., Mishan'kin, B.N., 1987. [Transparent nutrient medium for culturing Francisella tularensis]. Antibiot. Med Biotekhnol 32, 133–137.
Radlinski, L.C., Brunton, J., Steele, S., Taft-Benz, S., Kawula, T.H., 2018. Defining the metabolic pathways and host-derived carbon substrates required for francisella tularensis intracellular growth. MBio 9.
Rytter, H., Jamet, A., Ziveri, J., Ramond, E., Coureuil, M., Lagouge-Roussey, P., Euphrasie, D., Tros, F., Goudin, N., Chhuon, C., Nemazanyy, I., de Moraes, F.E., Labate, C., Guerrera, I.C., Charbit, A., 2021. The pentose phosphate pathway constitutes a major metabolic hub in pathogenic Francisella. PLoS Pathog. 17, e1009326.
Saitou, N., Nei, M., 1987. The neighbor-joining method: a new method for reconstructing phylogenetic trees. Mol. Biol. Evol. 4, 406–425.
Schulze, C., Heuner, K., Myrtennas, K., Karlsson, E., Jacob, D., Kutzer, P., K, G.R., Forsman, M., Grunow, R., 2016. High and novel genetic diversity of Francisella tularensis in Germany and indication of environmental persistence. Epidemiol. Infect. 144, 3025–3036.
Seiwald, S., Simeon, A., Hofer, E., Weiss, G., Bellmann-Weiler, R., 2020. Tularemia goes west: epidemiology of an emerging infection in Austria. Microorganisms 8.
Shibata, K., Shimizu, T., Nakahara, M., Ito, E., Legoux, F., Fujii, S., Yamada, Y., Furutani-Seiki, M., Lantz, O., Yamasaki, S., Watarai, M., Shirai, M., 2022. The intracellular pathogen Francisella tularensis escapes from adaptive immunity by metabolic adaptation. Life Sci. Alliance 5.
Sundell, D., Uneklint, I., Ohrman, C., Salomonsson, E., Karlsson, L., Backman, S., Naslund, J., Sjodin, A., Forsman, M., Appelt, S., Drechsel, O., Jacob, D., Heuner, K., Myrtennas, K., 2020. Complete Genome Sequence of Francisella tularensis subsp. holarctica Strain A271_1 (FDC408), Isolated from a Eurasian. Beaver (Castor Fiber). Microbiol Resour. Announc 9.
Svensson, K., Back, E., Eliasson, H., Berglund, L., Granberg, M., Karlsson, L., Larsson, P., Forsman, M., Johansson, A., 2009a. Landscape epidemiology of tularemia outbreaks in Sweden. Emerg. Infect. Dis. 15, 1937–1947.
Svensson, K., Granberg, M., Karlsson, L., Neubauerova, V., Forsman, M., Johansson, A., 2009b. A real-time PCR array for hierarchical identification of Francisella isolates. PLoS One 4, e8360.
Svensson, K., Larsson, P., Johansson, D., Bystrom, M., Forsman, M., Johansson, A., 2005. Evolution of subspecies of Francisella tularensis. J. Bacteriol. 187, 3903–3908.
Tlapak, H., Koppen, K., Rydzewski, K., Grunow, R., Heuner, K., 2018. Construction of a new phage integration Vector pFIV-Val for Use in different francisella species. Front Cell Infect. Microbiol 8, 75.
Tomaso, H., Hotzel, H., Otto, P., Myrtennas, K., Forsman, M., 2017. Antibiotic susceptibility in vitro of Francisella tularensis subsp. holarctica isolates from Germany. J. Antimicrob. Chemother. 72, 2539–2543.
Tully, B.G., Huntley, J.F., 2020. Mechanisms affecting the acquisition, persistence and transmission of francisella tularensis in ticks. Microorganisms 8.
Unthan, S., Baumgart, M., Radek, A., Herbst, M., Siebert, D., Bruhl, N., Bartsch, A., Bott, M., Wiechert, W., Marin, K., Hans, S., Kramer, R., Seibold, G., Frunzke, J., Kalinowski, J., Ruckert, C., Wendisch, V.F., Noack, S., 2015. Chassis organism from Corynebacterium glutamicum–a top-down approach to identify and delete irrelevant gene clusters. Biotechnol. J. 10, 290–301.
Vogler, A.J., Birdsell, D., Price, L.B., Bowers, J.R., Beckstrom-Sternberg, S.M., Auerbach, R.K., Beckstrom-Sternberg, J.S., Johansson, A., Clare, A., Buchhagen, J.L., Petersen, J.M., Pearson, T., Vaissaire, J., Dempsey, M.P., Foxall, P., Engelthaler, D. M., Wagner, D.M., Keim, P., 2009a. Phylogeography of Francisella tularensis: global expansion of a highly fit clone. J. Bacteriol. 191, 2474–2484.
Vogler, A.J., Birdsell, D., Wagner, D.M., Keim, P., 2009b. An optimized, multiplexed multi-locus variable-number tandem repeat analysis system for genotyping Francisella tularensis. Lett. Appl. Microbiol 48, 140–144.
Wick, R.R., Judd, L.M., Gorrie, C.L., Holt, K.E., 2017. Unicycler: Resolving bacterial genome assemblies from short and long sequencing reads. PLoS Comput. Biol. 13, e1005595.
Witt, N., Andreotti, S., Busch, A., Neubert, K., Reinert, K., Tomaso, H., Meierhofer, D., 2020. Rapid and culture free identification of francisella in hare carcasses by high-resolution tandem mass spectrometry proteotyping. Front Microbiol 11, 636.
Wittwer, M., Altpeter, E., Pilo, P., Gygli, S.M., Beuret, C., Foucault, F., Ackermann-Gaumann, R., Karrer, U., Jacob, D., Grunow, R., Schurch, N., 2018. Population Genomics of Francisella tularensis subsp. holarctica and its implication on the eco-epidemiology of tularemia in Switzerland. Front Cell Infect. Microbiol 8, 89.
Ziveri, J., Barel, M., Charbit, A., 2017a. Importance of metabolic adaptations in Francisella Pathogenesis. Front Cell Infect. Microbiol 7, 96.
Ziveri, J., Tros, F., Guerrera, I.C., Chhuon, C., Audry, M., Dupuis, M., Barel, M., Korniotis, S., Fillatreau, S., Gales, L., Cahoreau, E., Charbit, A., 2017b. The metabolic enzyme fructose-1,6-bisphosphate aldolase acts as a transcriptional regulator in pathogenic Francisella. Nat. Commun. 8, 853.